

Manuscript Number: MARSYS-D-13-00079R1

Title: ON THERMOHALINE STRUCTURE AND CIRCULATION OF THE WESTERN LARGE ARAL SEA
FROM 2009 TO 2011: OBSERVATIONS AND MODELING

Article Type: Research Paper

Keywords: Aral Sea; circulation; thermohaline structure

Corresponding Author: Mr. Alexander Izhitskiy,

Corresponding Author's Institution: P.P. Shirshov Institute of Oceanology

First Author: Alexander Izhitskiy

Order of Authors: Alexander Izhitskiy; Peter Zavialov; Elena Roget; Huei-Ping Huang; Abulgazi Kurbaniyazov

Abstract: The shrinkage of the Aral Sea in the second half of the past century has significantly affected the hydrophysical regime of the lake. The objective of this paper is to report on a hydrological structure and circulation of the today's Aral Sea based on both direct field observations and modeling results. We focus on the results of three field surveys to the Aral Sea which took place in the period from 2009 to 2011. In addition, series of numerical experiments using Princeton Ocean Model adapted to the Aral Sea was undertaken to investigate the contributions from bathymetry and water stratification in the formation of the basin scale circulation.

The hydrological structure of the Aral's western basin in autumn season exhibited a three-layered pattern with two local salinity maxima, separated by a fresher intermediate layer. According to direct observations, water circulation in the surface layer has anti-cyclonic character, while circulation in the bottom layer has cyclonic sign under the predominant northerly winds. The simulation experiments demonstrated clearly that the main cause of the anti-cyclonic circulation in the surface layer of the lake is the "asymmetric" bathymetry with broad shallow area along the eastern coast and relatively steep and deep western slope. However, strong stratification is a necessary condition for the formation of the cyclonic circulation gyre in the bottom layer.

1
2 **ON THERMOHALINE STRUCTURE AND CIRCULATION OF THE WESTERN**
3 **LARGE ARAL SEA FROM 2009 TO 2011: OBSERVATIONS AND MODELING**

4
5 **A.S. Izhitskiy^a, P.O. Zavialov^a, E. Roget^b, H.-P. Huang^c, A.K. Kurbaniyazov^{d,e}**

6
7 a – P.P. Shirshov Institute of Oceanology, 36, Nakhimovskiy Prospect Ave., Moscow,
8 117997, Russia

9 b – University of Girona, PII. Campus Montilivi, Girona, 17071, Catalonia, Spain

10 c – Arizona State University, Tempe, AZ 85287-6106, USA

11 d – Ahmet Yassau International Kazakh-Turkish University, Turkestan, Kazakhstan

12 e – Quaraqualpaq State University, Nukus, Uzbekistan

13
14 **1. Introduction**

15
16 Until 1960, the Aral Sea, a terminal lake in Central Asia, was the World's fourth largest
17 inland waterbody by area. Mainly because of intensive water diversion from the Amu-Darya and
18 Syr-Darya rivers for irrigation, the Aral Sea began to shrink dramatically in 1960. In comparison
19 with pre-desiccation state, to the date of this writing, the overall level drop was about 26 m.
20 Nowadays, the Aral Sea has lost more than 90% percent of its volume (Zavialov et al, 2012).
21 The shrinkage resulted in profound changes of the lake's ecosystem and desertification of the
22 surrounding areas. The ecological crisis of the Aral Sea has attracted attention of mass media and
23 international scientific community. Moreover, the significance of the ongoing changes of the
24 Aral Sea is not limited to the applied, regional aspects. The lake can be thought of as a “natural
25 laboratory”, where the evolution of a large inland water body under anthropogenic intervention
26 through diversions of the river runoff can be investigated. Such an investigation could be also
27 instructive with respect to other similarly exposed regions all over the World.

28 The Aral Sea was covered by data relatively well in the times of the former USSR.
29 However, during the period of the most rapid changes of the Aral Sea hydrological system, i.e.,
30 the 1990s, the in situ observations in the lake were extremely sparse. The reason was the well-
31 known political and economic troubles following the collapse of the USSR, as well as the
32 complete cessation of the navigation in the Aral Sea at advanced stages of desiccation. This
33 resulted in a practically total lack of data about many basic characteristics of the rapidly
34 changing Aral Sea environment at the beginning of the new millennium. Most works published
35 after the early 1990s were confined to either modeling or remote sensing (e.g., Ginsburg et al,
36 2002). In 2002, the Shirshov Institute of Oceanology of the Russian Academy of Sciences
37 (SIORAS) launched a long-term program of field research and monitoring of the Aral Sea. The
38 field observations are conducted in collaboration with a number of other institutions in Russia
39 and Central Asia's states of Uzbekistan and Kazakhstan.

40 The objective of this article is to report on a hydrological regime and circulation of the
41 today's Aral Sea based on both direct field observations and some modeling results. The paper is
42 centered on the results of the 3 latest field surveys of SIORAS to the Aral Sea which took place
43 in August, 2009, September, 2010 and November, 2011. Similar data collected in the surveys
44 since 2002 through 2008 have been published previously (e.g., Zavialov, 2005, Zavialov, 2009),
45 and in this paper we recall them only briefly, mainly focusing on the results of 2009, 2010 and
46 2011 presented here for the first time.

47 The paper also reports on numerical model simulations of the Aral Sea circulation. The
48 properties of basin-scale circulation gyres in major lakes have been subject of a number of
49 previous studies. For example, Schwab and Beletsky (2003) investigated relative importance of
50 different mechanisms to explain the large-scale gyres in Lake Michigan and found that wind
51 stress curl and the baroclinic effects were the dominant factors, but the topographic effects were
52 also significant. The effects of bathymetry on circulation patterns in lakes have been addressed in
53 early works by Shtokman (1953). Pickett and Bermick (1977) studied Lake Ontario during the
54 stratified season and reported a circulation consisting of a major counterclockwise gyre
55 complemented with a smaller clockwise gyre in the northern part of the lake. In the case of Great
56 American Lakes (whose geographic and morphological settings are in some respects similar to
57 those of the Aral Sea), Beletsky et al. (1999) argued that the observed cyclonic circulation
58 pattern was associated with the vorticity of the wind stress field. However, smaller lakes tend to
59 manifest two-gyre rather than a single gyre circulation patterns. For example, double gyre
60 circulations were observed in the Lake Tahoe (e.g., Strub and Powell, 1986, Rueda et al., 2005).
61 A combination of an anticlockwise gyre and a weaker clockwise gyre has also been reported for
62 the Lake Kinneret (Marti and Imberger, 2008). Shimizu et al. (2007) studied the Lake Biwa
63 during the stratified period and identified anticyclonic sub-basin scale gyres. Beletsky et al.
64 (2006) concluded that in general, the density effects added to the wind action led to a more
65 complex circulation pattern in lakes.

66 In the present paper, we investigate the circulation of today's hyperhaline, highly
67 stratified Aral Sea and attempt to quantify the underlying mechanisms based on in situ
68 measurements as well as numerical modeling. Information about geographical and physical
69 conditions of the Aral Sea as well as the historical background of the problem are summarized in
70 Section 2. Details of the field campaigns and the model experiments are given in Section 3. The
71 thermal and salinity structures across the main lobe of the Aral Sea are presented and analyzed in
72 the Section 4. Investigation of water circulation based on observations is analyzed in Section 5
73 and numerical modeling results are presented in Section 6. Conclusions are drawn in Section 7.

74

75 **2. Geographic settings of the lake**

76

77 The Aral Sea in its original, pre-desiccation state was a brackish lake whose salinity
78 varied only slightly around 10 g/kg. The minimum values were mainly associated with river
79 mouth areas, while the highest were distributed in the deepest western part of the basin. The
80 seasonal cycling of salinity was largely insignificant (Kosarev, 1975). In contrast with the
81 salinity values, the temperature demonstrated strong spatial and temporal variability. High
82 seasonal range of SST (about 25°C) and steep thermocline with maximum vertical gradients up
83 to 1°C/m were characteristic for the lake in the summer season (Bortnik and Chistyeva, 1990).
84 Therefore, the vertical stratification of the pre-desiccation Aral Sea was mainly controlled by the
85 temperature regime rather than salinity. Cooling of the upper layer of the lake in autumn caused
86 convection movement throughout the water column down to the bottom. This factor provided for
87 seasonal mixing of the water column and prevented the formation of pronounced density
88 stratification. These features of hydrological structure were also typical for the Aral Sea during
89 the early stages of the desiccation (Bortnik and Chistyeva, 1990).

90 The thermohaline structure of the Aral Sea at the present stage of advanced desiccation is
91 much different from the pattern observed in the middle of the last century. Starting from 1960, a
92 continuous increase of salinity has been observed. The salinity growth was essentially uniform

93 across different parts of the lake until the late 1990s, when the Large Aral Sea divided into two
94 basins, i.e., the Western Large Aral Sea and the Eastern Large Aral Sea, connected through a
95 narrow strait formed due to intensive bottom erosion during the shrinking period (Roget et al.,
96 2009). Since then, salinity growth in the broad and shallow eastern basin became more intense
97 than in the relatively deep and less extensive western basin. The differences in TS-characteristics
98 of eastern and western basins created strong horizontal salinity gradients. Also, the penetration of
99 much saltier water from the eastern basin to the west basin through the connecting strait resulted
100 in strong salinity and, hence, density stratification in the western basin of the Large Aral Sea. As
101 observed in surveys to the Aral Sea conducted by SIORAS since 2002, two archetypes of
102 hydrological structure of the western basin in fall and summer seasons were persistent through
103 the last decade. The first type is characterized by “two-layered” structure with salinity minimum
104 in the upper mixed layer, followed by steep halocline and salinity maximum in the bottom layer.
105 The other type of stratification exhibits the “three-layered” pattern with two salinity maxima, one
106 in the upper mixed layer and one in the bottom layer, separated by a layer of fresher water. In
107 this case, vertical stability is maintained by steep thermocline. It has been hypothesized that
108 these features of hydrological structure of the western basin were determined by two
109 mechanisms, sometimes termed as *convective* and *advective* (e.g. Zavialov, 2005, Zavialov et al,
110 2012). The convective mechanism provides for salinity growth in the upper mixed layer by
111 means of intense evaporation from the surface of the lake in the warm season. In this case, the
112 water column retains stable density stratification until the beginning of the autumn cooling and
113 subsequent development of the vertical convection. On the other hand, the local salinity
114 maximum in the bottom layer is connected with the advective mechanism, which implies the
115 water inflow from the eastern basin through the connecting strait. Direct measurements of 2004
116 yielded estimate of this inflow at about 1500 m³/s [Zavialov, 2005]. The much saltier and denser
117 waters from the east fill the bottom layer of the western basin, providing for extremely stable
118 density stratification. The TS-analysis based on CTD-measurements obtained in autumn 2002
119 showed that 9 to 11% of water in the bottom layer of the western basin had originated from the
120 eastern basin (Zavialov, 2005). The resulting high vertical gradients of density largely suppress
121 the autumn/winter convection. The frequent features of the present day Aral Sea such as the
122 temperature inversions, anoxia and hydrogen sulfide contamination in the bottom layer are
123 manifestations of reduced mixing. In contrast with the convective mechanism, the advective one
124 exhibits strong interannual variability (Zavialov et al., 2012).

125 The circulation of the pre-desiccation Aral Sea had not been thoroughly explored because
126 of relatively small number of direct measurements. However, even the early researchers pointed
127 out that the lake’s mean circulation pattern appeared to have the anticyclonic direction (Berg,
128 1908, Zhdanko, 1940). This is rather unusual, given that the neighboring inland seas, such as the
129 Caspian Sea, the Black Sea and the Azov Sea, belonging to the same latitudinal belt and exposed
130 to similar predominant winds, all maintain cyclonic character of their large-scale circulation. The
131 early researchers of the Aral Sea hypothesized that this peculiar feature of the Aral Sea’s surface
132 circulation resulted from the impact of river inflows (Berg, 1908, Zhdanko, 1940). This
133 hypothesis was based on simplified calculations such as the geostrophic method, as well as
134 analyses of plankton concentration as a tracer for the currents. Later on, basing on theoretical
135 works by V.B. Shtokman, A.I. Simonov attributed the anticyclonic sign of Aral Sea’s surface
136 circulation to a combined effect of the predominant northerly winds inhomogeneously
137 distributed over the basin, and the lake’s bathymetry (Shtokman, 1953, Simonov, 1954).
138 Furthermore, some model results showed that the surface circulation can switch to cyclonic

139 under the conditions of southerly winds (Bortnik, Chistyayeva, 1990). In addition, the baroclinic
140 motions of denser waters from relatively shallow eastern part of the lake to the western trench
141 have been documented even before the onset of the desiccation (Simonov, 1962).

142 Recent studies (e.g. Zavialov, 2005) pointed out that the sign of circulation gyre in the
143 Aral Sea's surface layer did not change during the desiccation. Indeed, despite the drastic
144 changes in the bathymetry and geometry of the sea, the basin-scale surface circulation in the
145 Western Large Aral Sea retained the anticyclonic character. In this paper, we report new data
146 supporting this notion and discuss possible mechanisms responsible for the observed character of
147 the present day circulation. During the field campaigns carried out during 3 consecutive years,
148 measurements of current velocity and wind stress were performed on site at high temporal
149 resolution. This allowed analyzing the short-time response of the lake to the wind variability. On
150 the other hand, because the mean wind conditions during the field experiments were rather close
151 to the climatic regime (Bortnik and Chistyayeva, 1990) the recorded data can also be used to
152 validate the results of numerical model forced by climatic winds.

153 154 **3. Data and methods**

155 156 *a) Observations*

157 The research area is situated in the deepest portion of the western basin of the Aral Sea
158 (Fig. 1). Each of the field surveys (August, 2009, September, 2010 and November, 2011)
159 included CTD-profiling, deployment of mooring stations with current meters and pressure
160 gauges, and water sampling. A summary of the measurements is given in Table 1.

161 Surface-to-bottom CTD-profiling was performed at 4 Hz sampling rate at regular section
162 across the western basin (Fig. 1), using *SBE 19plus SeaCat* profiler. As known, general problem
163 with interpreting CTD data collected from the Aral Sea is linked with the salt composition of the
164 water, which is significantly different from the ocean water. In consequence, the relation
165 between the electric conductivity and salinity is also different. Therefore, we applied the
166 following procedure to infer the salinity from the original CTD data. First, the true salinities of
167 the collected water samples were obtained chemically in laboratory through "dry residue"
168 method. Then, the corresponding "pseudo salinity" values S_{ctd} , i.e., those computed through the
169 standard oceanic relation, were extracted from the CTD data, and linear regression between the
170 laboratory salinity and CTD-derived pseudo salinity values was constructed. The linear relation
171 obtained thereby was then used to convert the entire set of CTD data to the "true" salinity. This
172 conversion was done on an individual basis for each cruise. As an example, we give here the
173 following regression based on chemically analyzed water samples collected in September, 2010:

$$174
175 S_{real} = 1.107 * S_{ctd} + 18.48 \quad (1)$$

176
177 Mooring stations equipped with current meters, one near the surface (depth 3-5 m) and
178 one in the near bottom layer (depth 20-22 m) at each mooring, as well as pressure gauge at the
179 bottom, were deployed at the locations shown in Figure 1. Mooring station "W" was installed at
180 the western slope of the basin, while the station "E" was positioned at the eastern slope.
181 Additionally, in September, 2010, a northern mooring station "N" was placed a 9 km to the
182 north. Each of the moorings remained in operation for 4-5 days following the installation,
183 collecting the data every 1 min. Also, a portable automatic meteorological station, continuously

184 recording the wind speed and other principal meteorological parameters at 10 min sampling rate,
185 was installed near the mooring site “W”. The time series of the sea level variability, surface and
186 bottom currents obtained at the moorings were then filtered with 10-min wide moving window.
187 The lagged correlations between these parameters and wind stress were calculated to investigate
188 the relations between the wind stress as a forcing factor and the water circulation as a basin
189 response. Finally, the absolute elevation of the Aral Sea surface above the ocean level was
190 determined through direct geodesic leveling using a nearby triangulation beacon located at the
191 western bank of the western basin.

192 193 *b) Model specifics*

194 Apart from analysis of the *in situ* observations, we used the obtained data to implement
195 model simulations in order to investigate the origin of the anticyclonic character of water
196 circulation in the surface layer of the lake under the predominant northeasterly winds. A series of
197 numerical experiments were performed by using the 3D Princeton Ocean Model (POM)
198 (Mellor, 1992) adapted to the Aral Sea was undertaken at the University of Girona. The
199 bathymetry of the western basin of the Aral Sea (Fig. 2, left panel) was digitized in a grid with
200 211 nodes along NS direction with a resolution of 967.02 m and 173 nodes along the EW
201 direction with a resolution of and 538.67 m. For the vertical coordinate a total of 17 equidistant
202 sigma levels were considered. Maximum depth of the numerical model of the lake in 2010 was
203 39 m and the mean of 4 m.

204 The duration of each model experiment was 12 days and the results presented correspond
205 to the mean values computed between the days 9 and 12. The model was forced by a constant
206 and spatially uniform 3 m/sec NE wind, which is in agreement with the climatic wind conditions
207 over the Aral Sea region (Bortnik and Chistyayeva, 1990). Wind stresses were computed
208 according to $\tau = \rho_a C_D V^2$, the drag coefficient C_D being parameterized according to Hasselmann
209 (1988). Similar approach is considered for the bottom stress where the drag coefficient was
210 calculated in order to fit the velocities at the first grid points nearest the bottom to the law of the
211 wall, considering a bottom roughness of 0.01 m. Zero normal velocities were used as the lateral
212 boundary conditions. For all simulations the heat flux at all the boundaries was set to zero.

213 As mentioned above, the bathymetry is thought to be one of the main factors determining
214 the sign of water circulation in the Aral Sea. Despite the enormous morphometric changes
215 accompanying the desiccation, the bathymetry of the lake retained its principal pattern, also
216 characteristic for the pre-desiccation state: the western slope is very steep, while the eastern
217 slope is much gentler. It has been hypothesized by (Simonov, 1954) that such an asymmetry
218 could be one of the factors determining the anticyclonic sign of the circulation gyre. To verify
219 this statement, we also repeat model experiments with the bathymetry inverted with respect to
220 the longitudinal axis of the basin (Fig. 2, right panel) and look at the changes which the inversion
221 produces in the circulation regime.

222 For each experiment, either stratified or non-stratified initial conditions were imposed. In
223 the former case, the “real” stratification inferred from CTD measurements of 2010 were used
224 (Fig .3). The specific equation of state (i.e., the relation between temperature, salinity and
225 density) recently obtained by (Gertman and Zavialov, 2011) for the present-day Aral Sea was
226 used in the model instead of the oceanic equation of state which is not valid for the conditions of
227 the Aral Sea. For the simulations with non-stratified conditions, we used a constant temperature
228 of 15°C and a constant salinity of 106 g/kg.

229 In numerical simulation, we focused on two cases: *unstratified* and *stratified*. Each of
230 these cases involved two experiments with the real and inverted bathymetry. This approach
231 allows to investigate the individual contribution from each of the factors in the formation of
232 basin scale circulation.

233 Accordingly, in total, we performed 4 model experiments: 1) real bathymetry, non-
234 stratified conditions, 2) real bathymetry, stratified conditions, 3) inverted bathymetry, non-
235 stratified conditions, and 4) inverted bathymetry, stratified conditions.

236 237 **4. Thermohaline structure**

238
239 Results of the measurements in the western basin of the Aral Sea in August, 2009 are
240 depicted in Fig. 4. The upper mixed layer with temperature about 24°C and salinity around 113.5
241 g/kg extended up to 13 m depth in the eastern part of the basin, and 6 to 7 m depth in the western
242 part. Strong seasonal thermocline with vertical gradients of temperature up to 2.2°C/m separated
243 the upper mixed layer and the intermediate layer with the local minima of salinity and
244 temperature (at 5.5°C and 110.5 g/kg, respectively). Beneath 25 m depth, there was a bottom
245 layer characterized by temperature inversion and local salinity maximum. Thus, the thermohaline
246 structure of the western basin in August, 2009 exhibited a three-layered pattern with two salinity
247 maxima separated by relatively fresh intermediate layer. Hypothetically, the presence of two
248 salinity maxima resulted from activity of the two forming mechanisms, mentioned above as
249 advective and convective. The reduction of difference between the surface and the bottom
250 salinity values compared with that observed in similar measurements of 2008 (Zavialov, 2009)
251 may indicate weakening of the advective mechanism. Indeed, the eastern basin has shrunk
252 almost completely during the summer of 2009, so the volume of the interbasin exchange and
253 thus the replenishment of the bottom high salinity level must have decreased.

254 The character of thermohaline structure, observed in the western basin in September, 2010
255 (Fig. 5), was generally similar to that in August, 2009. Three layers, including surface and
256 bottom local salinity maxima separated by relatively fresh intermediate water, were again seen.
257 The upper mixed layer extended down to 14.5 m depth with average temperature values about
258 19°C and average salinity values around 117 g/kg. The steep thermocline with temperature drop
259 as large as of 11°C over only 3 m of the column was located below upper mixed layer. The core
260 of relatively fresh intermediate layer with temperature values below 7°C and salinity values
261 below 113 g/kg was located under the thermocline. The upper boundary of the bottom layer was
262 located at around 28 m depth, from where salinity values started to increase rapidly downward to
263 the bottom. Also, the bottom salinity maximum was accompanied by typical temperature
264 inversion with temperature growth by up to 4°C, see also Fig. 6. The difference in salinity values
265 between the surface and the bottom maxima constituted 15 g/kg, which is much higher than that
266 observed in 2009. According to the available satellite data (Soloviov, pers. com.), the volume of
267 water in the eastern basin has grown substantially during the autumn/winter season of
268 2009/2010, and the exchanges between the basins resumed.

269 The new results reported above, therefore, appear to be consistent with the hypothesis
270 moved forward in a number of previous studies: the stratification of the western basin depends
271 strongly on the intensity and characteristics of salt exchange between the eastern and the western
272 basins of the sea through the connecting strait. When the eastern basin is either small (situation
273 of 2009) or not as much saltier than the western one, and the salt exchange is reduced, the
274 stratification of the western basin relaxes and tends to take a “two-layered” structure, with only

275 one salinity maximum in the upper layer following intense summer evaporation. The profile of
276 2009 (Fig. 6) appears to correspond to this situation, followed by restoration of “three-layered”
277 pattern with well-developed salinity maximum at the bottom after the exchange resumed in 2010
278 (Fig. 6). The bottom salinity decreased again after the exchanges ceased again in 2011.

279 On the other hand, it has to be kept in mind that there is no data on the salinity of the
280 eastern basin after its re-plenishment with Amu-Darya water in 2010, and it is not impossible
281 that, at present, it may be actually lower than that in the western basin. Nevertheless, the newly
282 obtained data on the thermohaline structure appear to support the concept of the exchanges with
283 the eastern basin as the principle controller of stratification in the western basin.

284 285 **5. Water circulation: observations**

286
287 Some general ideas about nowadays features of water circulation in the Aral Sea could be
288 obtained basing on the analysis of observations as well as model experiments.

289 Fig. 7 depicts the wind forcing conditions over the western basin during the periods of
290 measurements in the 3 field campaigns. In all 3 cases, the winds blew approximately along the
291 main axis of the basin during the most part of the observations. During the most significant wind
292 events, the wind stress was directed to the south (except the conditions observed in November,
293 2011). The northerly and northeasterly winds prevail over the Aral Sea basin within most of the
294 year (e.g., Bortnik and Chistyeva, 1990). Thus, the wind conditions during the measurements
295 were close to the climatic regime.

296 Fig. 8 (left panel) shows the results of direct measurements of current velocities and
297 directions, as well as sea level variability, conducted in the central part of the western basin in
298 August, 2009. The near-surface current at the eastern slope of the basin has general southward
299 alongshore direction during almost the entire period of measurements. The highest velocity
300 values were observed on August 22 after an intense southward wind burst. The near-surface
301 currents at the western slope did not exhibit equally well-defined character, although showing
302 development of northward currents corresponding to northern wind events with some time lag.
303 The sea level rise at the western slope, observed from August 22 to the end of the measurement
304 period, apparently was also caused by the northern wind forcing. The reason of the sharp
305 increase and then change of sign of the current velocity on day 232 is unclear. Hypothetically,
306 that could be a manifestation of seiches, which is believed to be a typical feature of the today’s
307 Aral Sea circulation (e.g., Zavialov et al, 2012).

308 Fig. 8 (right panel) exhibits the result of similar measurements, conducted in the western
309 basin in September, 2010. The atmospheric forcing during the survey generally was more intense
310 than that in the survey of 2009 (Fig. 7). Surface currents at the eastern slope reached the values
311 of 25 cm/s being directed to the south-southwest during the entire measurements period. At the
312 same time, surface currents at the western slope reached values around 45 cm/s with north-
313 northwestward direction. The most significant event of the northerly winds observed in the
314 beginning of the measurements period was accompanied by the sea level rise along the western
315 bank.

316 Results of current measurements conducted in the western basin during the surveys
317 demonstrate similar features. Despite the relative shortness of observations and some differences
318 in wind forcing for different observation periods, we can conclude that the general directions of
319 water fluxes were quite pronounced, namely, the northward direction for the surface current of
320 the western slope, and southward directions for the surface currents along the eastern shore. This

321 fact was observed in all the 3 surveys (2009, 2010, and 2011, Fig. 8, 9). Similarly, there were
322 predominant directions of the bottom currents at the basin slopes: the current was southward at
323 the western slope, and mainly northward at the eastern slope.

324 The observed features allow to conclude, that, despite the profound changes in
325 geographical conditions of the region and catastrophic decrease of sea volume, water circulation
326 in the surface layer of the Aral Sea remains anti-cyclonic, while circulation in the bottom layer
327 still retains the cyclonic character.

328 Some insight into the mechanisms of the basin response to the wind forcing can be
329 obtained through the analysis of time-lagged correlations between the components of wind
330 stress, currents and sea level anomaly. To this end, we analyze here the measurements conducted
331 in September, 2010. We are mainly interested in the basin response to the climatic wind stress, to
332 which the observations of September 2010 were probably the closest proxy. The northern
333 component of the wind stress exhibits positive correlation with northern component of the
334 surface current at the eastern slope for all temporal lags considered (Fig. 10a). In the initial phase
335 of the response to a wind event, the northern component of the surface current at the western
336 slope has positive correlation (maximum $r=0.52$ for the lag of 6.1 hrs) with northern component
337 of the wind stress, which then turns to be negative after about 33 hours from the beginning
338 (maximum $r= -0.66$ for the lag of 48.5 hrs, Fig. 10c). At the same time, there is negative
339 correlation between the northern component of the surface current at the eastern slope and sea
340 level anomaly above the western slope with any time lag (Fig. 10b). The northern component of
341 the surface current at the western slope exhibits high positive synchronous correlation ($r=0.74$
342 for the lag of 0 hrs) with the sea level anomaly at the western slope (Fig. 10d). For large lags,
343 this connection transforms to negative and very high ($r=0.91$ for the lag of 50 hrs). This
344 transformation of the positive correlations to negative, as shown in Fig. 10c and Fig. 10d, points
345 towards the compensative character of the alongshore surface current under the western slope.
346 Indeed, this means that the surface currents at the western bank flow “against” the wind, and
347 reacts not on wind itself but, rather, on the circulation and the level changes across the sea once
348 they are established after some time following wind event. Bottom currents along the slopes of
349 the basin demonstrate the well-pronounced negative correlation ($r =0.87$) with the maximum at
350 about 40 hrs time lag (Fig. 10e). Surface currents in the western and eastern parts of the sea show
351 negative correlations with each other for any lag, but the maximum correlation coefficient $r=-0.7$
352 corresponds to the lag 37.5 hrs. Together with the measurement data shown in Fig. 8 (right
353 panel) this suggests the existence of anti-cyclonic gyre in the surface layer and cyclonic flow in
354 the bottom.

355 As mentioned above, the first explanation of the anti-cyclonic character of the Aral Sea’s
356 surface circulation was proposed by (Simonov, 1954), who attributed it to the peculiar
357 morphometry of the lake acting together with inhomogeneous wind stress. Presently, the
358 geographical conditions of the Aral Sea, pointed out by A.I. Simonov 59 years ago have
359 changed. The transverse scale of the basin (e.g. about 25 km in 2010) reduced by an order of
360 magnitude, so the inhomogeneous distribution of wind stress over the sea probably no longer has
361 significant influence. However, the peculiar bottom topography of the Aral Sea is still there. The
362 features of the circulation and its response to the wind forcing as observed in the measurements
363 reported in this study are likely to originate from this “asymmetry” in the bottom topography.
364 Shallow eastern areas of the sea respond more energetically to wind forcing, than the deep
365 western areas, so the sea level rise occurs near the western shore during the development of
366 southward along shore current near the eastern coast (Fig 10b). Accordingly, a northward

367 compensative current develops along the western shore after about 35 hrs since the wind event
368 (Fig. 10c). The sea level near the western coast begins to decrease (Fig. 10d) and the surface
369 circulation takes the anti-cyclonic character. Basing on measurements of 2010, the complete
370 period of the establishment of the anti-cyclonic flow in the western basin of the Aral Sea
371 following a northerly wind event can be estimated as about 40 hrs (Fig. 10f). Additional
372 confirmation of this concept of the Aral Sea will be presented below in the modeling section.

373 374 **6. Water circulation: modeling results**

375
376 In what follows, firstly, the unstratified case is presented in order to isolate the influence
377 of the bathymetry formation of the circulation. Then, we repeat the experiment for the stratified
378 case to determine the role of water column stratification in Aral's circulation features. We,
379 therefore, conduct two model experiments, one with the "real" bathymetry, and the other one
380 with the bathymetry "inverted" with respect to the long axis of the western basin

381 382 *a) Unstratified case*

383 The results of model experiment using the real bathymetry and the water column of
384 uniform density is shown in Fig. 11 (left panel). The corresponding pattern of the flow at surface
385 exhibits well-developed anticyclonic character of water circulation under the climatic
386 northeasterly winds. The southward surface flow coincides with the relatively shallow parts of
387 the basin, while the deep parts of the basin are mainly occupied by the northward surface flow.
388 The eastern shallow part of the basin is also characterized by the intensification of surface
389 currents.

390 Imposing of the inverted bathymetry in the case of unstratified basin yields the opposite
391 pattern, as far as the surface layer is concerned (Fig. 11, right panel). In this case, the flow at the
392 surface is organized as a cyclonic gyre with the intensified southward branch along the western
393 coast. Deeper parts of the "inverted" basin along the eastern shore exhibit a less intense
394 northward flow.

395 The velocity vectors for the bottom layer in this experiment are shown on Fig. 12 (left
396 panel). The general anticyclonic motion occupying the main lobe of the western Aral Sea in the
397 non-stratified case is observed to have the same sense at all depths throughout the water column.
398 The same pattern in the bottom layer is seen for the scenario with the inverted bathymetry, too
399 (Fig. 12, right panel). Hence, bathymetry inversion does not seem to have any significant
400 influence on the circulation character in the bottom layer.

401 402 *b) Stratified case*

403 Introducing a real stratification into the simulation experiments illustrates another
404 important effect. Fig. 13 shows the distribution of velocity vectors in the surface layer in the case
405 of stratified water column. Anticyclonic circulation character of surface circulation still complies
406 with real bathymetry (Fig. 13, left panel) while the cyclonic surface circulation results from the
407 inverted bathymetry (Fig. 13, right panel). A constant and uniform NE wind was used as a
408 forcing factor in both cases. Therefore, in the stratified case, the bathymetry pattern still
409 constitutes the dominant role in the formation of circulation character at the surface. The
410 bathymetry inversion alone led to the change of the circulation sign to the opposite under the
411 otherwise constant conditions, no matter whether the column was stratified or not. However, it
412 should be pointed out, that the velocity field in the stratified case is more complex than that for

413 the non-stratified scenario. In the stratified case, the circulation pattern includes smaller, sub-
414 basin scale gyres (anti-cyclonic for the real bathymetry and cyclonic for the inverted bathymetry)
415 occupying the central part of the basin (Fig. 13).

416 On the other hand, the introduction of stratification does affect significantly the
417 circulation character in the bottom layer of the basin, causing development of a cyclonic gyre
418 (Fig. 14). The dominance of cyclonic vorticity in the bottom layer was observed both in cases of
419 the real and inverted bathymetries and depended only on the presence of stratification. In the
420 case of real bathymetry, a clockwise gyre is observed in the central part of the western trench. In
421 this region, the sign of the circulation does not change from surface to bottom (Figs. 13, 14). In
422 addition, there are two well-developed smaller eddies in the northern and southern vicinities of
423 the central gyre (Figs. 13, 14). These smaller gyres are anti-cyclonic in the upper layer and
424 cyclonic in the lower layer. This “two-layered” character of the water circulation is apparently
425 caused by the presence of stratification. The location of the bottom cyclonic gyres is likely to be
426 sensible to the wind direction. *In situ* observations with better coverage in space and time will
427 help to clarify the question in the future.

428 **7. Conclusions**

- 430
431 1. During the study period, the hydrological structure of the Aral’s western basin in
432 autumn exhibited a three-layered pattern with two local salinity maxima, separated by
433 a fresher intermediate layer. As hypothesized in previous publications (e.g. Zavialov,
434 2005, Zavialov et al., 2012), the observed structure resulted from combined action of
435 two forming mechanisms, referred to as “convective” and “advective”.
- 436 2. The latter, connected with the water exchange between the western and the eastern
437 basins of the Large Aral Sea, is subject to significant interannual changes. Indeed, in
438 the summer of 2009, when the eastern basin had dried almost completely and the
439 interbasin exchange had practically ceased, the salinity values at the surface and in
440 the bottom were close to each other. Subsequently, the intensity of the interbasin
441 exchanges increased again, and in the autumn of 2011, the difference in salinity
442 between the surface and the bottom layers attained high values around 11 g/kg, while
443 the relatively fresh intermediate layer remained between the two salinity maxima.
- 444 3. Despite the profound changes in geographical and hydrological conditions of the lake,
445 water circulation in the deep western basin still retains its peculiar character, typical
446 for the Aral Sea in its pre-desiccation state. According to direct observations, water
447 circulation in the surface layer has anti-cyclonic character, while circulation in the
448 bottom layer is more complex but generally has cyclonic sign under the predominant
449 northerly winds.
- 450 4. We implemented a series of numerical model experiments with innovative approach
451 involving the “inverted” bathymetry of the lake along with the true one. These model
452 experiments, as well as the data analyses, helped to elucidate the origins of the anti-
453 cyclonic circulation establishment in the surface layer of the lake: the main reason for
454 this feature is the “asymmetric” bathymetry with broad shallow area along the eastern
455 coast and relatively steep and deep western part. Simulation experiments
456 demonstrated clearly that surface circulation switches to the opposite sign as soon as
457 the bathymetry is inverted with respect to the longitudinal axis of the basin.

458 5. According to modeling results, development of the circulation in the bottom layer of
459 the basin is intimately connected with the basin stratification and does not directly
460 depend on the bathymetry.

461

462 **Acknowledgements**

463

464 The authors gratefully acknowledge invaluable assistance of their collaborators and
465 colleagues from Tashkent Institute of Geology and Geophysics, as well as the support received
466 from EU FP7 Project CLIMSEAS (IRSES-2009N.247512), U.S. Civil Research and
467 Development Foundation (grant RUG1-2968-MO-10), and the Russian Ministry of Education
468 and Science.

469

470 **References**

471

472 Beletsky, D., Saylor, J.H., Schwab, D.J., 1999. Mean circulation in the Great Lakes. *J. Great*
473 *Lakes Res.* 25(1), 78–93.

474 Beletsky, D., Schwab, D., McCormick, M., 2006. Modeling the 1998–2003 summer circulation
475 and thermal structure in Lake Michigan. *J. Geophys. Res.* 111, C10010.

476 Berg, L.S., 1908. Aral Sea. An Attempt of Physical Geographic Description. *Izvestiya*
477 *Turkestanского Otdeleniya, Russian Geographic Society, St. Petersburg*, 5, 9, 580 pp. (in
478 Russian).

479 Bortnik, V.N. and Chistyayeva, S.P., 1990. Hydrometeorology and Hydrochemistry of the USSR
480 Seas. Vol. VII: The Aral Sea. *Gidrometeoizdat, Leningrad*, 196 pp. (in Russian).

481 Gertman, I., Zavialov, P.O., 2011. New equation of state for Aral Sea water. *Oceanology* 51,
482 367-369 (in Russian).

483 Ginzburg, A.I., Kostianoy, A.G., Sheremet, N.A., 2002. Thermal regime of the Aral Sea at
484 present time (1982-2000) based on satellite data. *Issled. Zemli iz Kosmosa* 4, 62-69 (in Russian)

485 Hasselman, S. 1988. The WAM model – a third generation ocean wave prediction model. *J.*
486 *Phys. Oceanogr.*, 18: 1775–1810.

487 Kosarev, A.N., 1975. Hydrology of Caspian Sea and Aral Sea. Moscow State University,
488 Moscow, 272 pp. (in Russian).

489 Marti, C.L., Imberger, J., 2008. Exchange between littoral and pelagic waters in a stratified lake
490 due to wind-induced motions: Lake Kinneret, Israel. *Hydrobiologia* 603, 25–51.

491 Mellor, G. L., 1992. User's guide for a three-dimensional, primitive equation, numerical ocean
492 model, *Progress in Atmospheric and Oceanic Sciences*, Princeton University, Princeton, 35 pp.

493 Pickett, R.L., Bermick, S., 1977. Observed resultant circulation of Lake Ontario. *Limnol.*
494 *Oceanogr.* 22, 1071-1076.

495 Roget, E., Zavialov, P.O., Khan, V.M., Muniz, M.A., 2009. Geodynamical processes in the
496 channel connecting the two lobes of the Large Aral Sea. *Hydrol. Earth Syst. Sci.* 13, 2265–2271.

497 Rueda, F.J., Schladow, S.G., Monismith, S.G., Stacey, M.T., 2005. On the effects of topography
498 on wind and the generation of currents in a large multi-basin lake. *Hydrobiologia* 532, 139–151.

- 499 Simonov, A.I., 1954. On origins of anticyclonic circulation of the Aral Sea waters.
500 Meteorologiya i Gidrologiya 2, 50-52 (in Russian).
- 501 Simonov, A.I., 1962. Origin of relatively high-salt waters in the western trench of the Aral Sea.
502 Tr. GOIN, 68, 103-117 (in Russian).
- 503 Shimizu, K., Imberger, J., Kumagai, M., 2007. Horizontal structure and excitation of primary
504 motions in a strongly stratified lake. Limnol. Oceanogr. 52(6), 2641–2655.
- 505 Shtokman, V.B., 1953. Impact of bottom topography and transversal wind variability to
506 horizontal circulation in the shallow sea or the water storage basin. Meteorologiya i Gidrologiya,
507 8, 16-22 (in Russian).
- 508 Schwab, D.J., Beletsky, D., 2003. Relative effects of wind stress curl, topography, and
509 stratification on large-scale circulation in Lake Michigan. J. Geophys. Res. 108, 3044.
- 510 Strub, P.T., Powell, T.M., 1986. Wind-driven surface transport in stratified closed basins: direct
511 versus residual circulations. J. Geophys. Res. 91, 8497-8508.
- 512 Zavialov, P.O., 2005. Physical Oceanography of the Dying Aral Sea. Springer-Verlag/Praxis,
513 Chichester, UK. 158 pp.
- 514 Zavialov, P.O., 2009. Physical oceanography of the Large Aral Sea, in: Kostianoy, A.G.,
515 Kosarev, A.N. (Eds.), Aral Sea Environment. Hdb Env Chem. Springer-Verlag, 123-146.
- 516 Zavialov, P.O., Arashkevich, E.G., Bastida, I., Ginzburg, A.I., Dikarev, S.N., Zhitina, L.S.,
517 Izhitskiy, A.S., Ishniyazov, D.P., Kostianoy, A.G., Kravtsova, V.I., Kudyshkin, T.V.,
518 Kurbaniyazov, A.K., Ni, A.A., Nikishina, A.B., Petrov, M.A., Sazhin, A.F., Sapozhnikov, P.V.,
519 Soloviov, D.M., Khan, V.M., Sheremet, N.A., 2012. The Large Aral Sea in the beginning of
520 century 21: Physics, Biology, Chemistry. Nauka, Moscow, 229 pp. (in Russian).
- 521 Zhdanko, S. M., 1940. Currents in the Aral Sea. Meteorologiya I Gidrologiya 1-2, 78-82 (in
522 Russian).

523 CAPTIONS

524 *Figure 1. The Aral Sea bathymetry for 1960 and for 2010, the Eastern Large Aral Sea is*
525 *shown schematically (upper panel). Schematic illustrating the locations of 6 CTD-stations on the*
526 *annual cross-section, two additional CTD-stations north, 3 mooring stations and meteorological*
527 *station (lower panel). The positions were retained during every field survey.*

528 *Figure 2. Bathymetry of the western basin used in the model simulations: real bathymetry*
529 *as of 2010 (left panel), inverted bathymetry (right panel).*

530 *Figure 3. Vertical profile of density, temperature and salinity used in the simulation, as*
531 *inferred from CTD measurements in September, 2010 .*

532 *Figure 4. Vertical distribution of temperature (°C, upper panel) and salinity (g/kg, lower*
533 *panel) along zonal cross-section of the western basin in August, 2009.*

534 *Figure 5. Vertical distribution of temperature (°C, upper panel) and salinity (g/kg, lower*
535 *panel) along zonal cross-section of the western basin. September, 2010.*

536 *Figure 6. Vertical profiles of salinity (g/kg), obtained in August, 2009, September, 2010,*
537 *and November, 2011 at the deepest station on the zonal cross-section.*

538 *Figure 7. Vector diagrams of wind stress during the field campaigns of 2009, 2010 and*
539 *2011.*

540 *Figure 8. Current velocities and directions, sea level variability and wind stress*
541 *variability, obtained from mooring recorders and meteorological station in August, 2009 (left*
542 *panel) and September, 2010 (right panel). From top to bottom: wind stress vectors (N/m^2), sea*
543 *level anomaly at station “W” (m), velocity vectors of surface current at station “W” (cm/s),*
544 *velocity vectors of bottom current at station “W” (cm/s), velocity vectors of surface current at*
545 *station “E” (cm/s), velocity vectors of bottom current at station “E” (cm/s).*

546 *Figure 9. Data from measurements of November, 2011. From top to bottom: wind stress*
547 *vectors (N/m^2), sea level anomaly at station “W” (m), velocity vectors of surface current at*
548 *station “W” (cm/s), velocity vectors of bottom current at station “W” (cm/s).*

549 *Figure 10. Lagged correlations between: northern component of the wind stress and*
550 *northern component of the surface current at station “E” (a), northern component of the surface*
551 *current at station “E” and the sea level anomaly at station “W” (b), northern component of the*
552 *wind stress and northern component of the surface current at station “W” (c), northern*
553 *component of the surface current at station “W” and the sea level anomaly at station “W” (d),*
554 *northern components of the bottom currents at stations “E” and “W” (e), northern components*
555 *of the surface currents at stations “E” and “W” (f).*

556 *Figure 11. Simulated surface circulation in case of non-stratified basin: real bathymetry*
557 *(left panel), inverted bathymetry (right panel).*

558 *Figure 12. Simulated water circulation in the bottom layer (29 m depth) in case of non-*
559 *stratified basin: real bathymetry (left panel) and inverted bathymetry (right panel).*

560 *Figure 13. Simulated surface circulation in the western basin in case of stratified basin:*
561 *real bathymetry (left panel), inverted bathymetry (right panel).*

562 *Figure 14. Simulated water circulation in the bottom layer (29 m depth) in case of*
563 *stratified basin in dependence of bathymetry: real bathymetry (left panel) and inverted*
564 *bathymetry (right panel).*

565

566 *Table 1. Field surveys and measurements used in this study*

567

Table1

[Click here to download Table\(s\): table1.docx](#)

Survey	CTD measurements	Mooring stations
August, 2009	<i>SBE 19plus SeaCat</i> 10 stations	<p>“E”: 19 – 23 August, 2009 velocity and pressure at 2 m depth - <i>Nortek Aquadopp</i>; bottom velocity – <i>SeaHorse</i>;</p> <p>“W”: 18 – 23 August, 2009 surface velocity – <i>SonTek Argonaut-MD</i>; bottom velocity – <i>SeaHorse</i>; sea level variability – <i>pressure gauge at bottom</i></p>
September, 2010	<i>SBE 19plus SeaCat</i> 11 stations	<p>“E”: 16 – 19 September, 2010 velocity and pressure at 2 m depth - <i>Nortek Aquadopp</i>; bottom velocity – <i>SeaHorse</i>;</p> <p>“W”: 14 – 19 September, 2010 surface velocity – <i>SonTek Argonaut-MD</i>; bottom velocity – <i>SeaHorse</i>; sea level variability – <i>pressure gauge at bottom</i></p> <p>“N”: 17 – 19 September, 2010 bottom velocity – <i>SeaHorse</i>; sea level variability – <i>pressure gauge at bottom</i></p>
November, 2011	<i>SBE 19plus SeaCat</i> 3 stations	<p>“W”: 3 – 5 November, 2011 days velocity and pressure at 2 m depth - <i>Nortek Aquadopp</i>; bottom velocity – <i>SeaHorse</i>;</p>

Figure2

[Click here to download high resolution image](#)

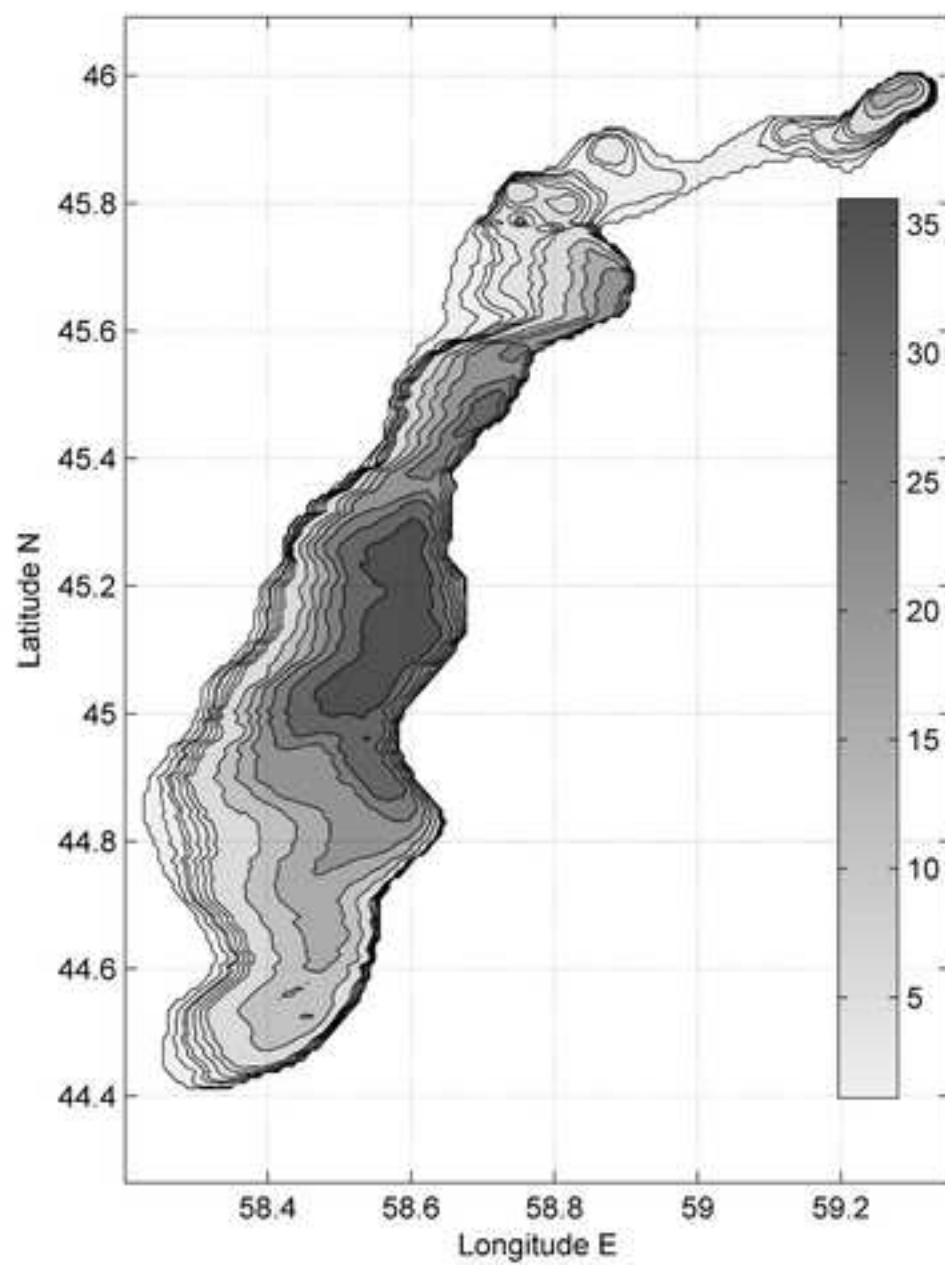
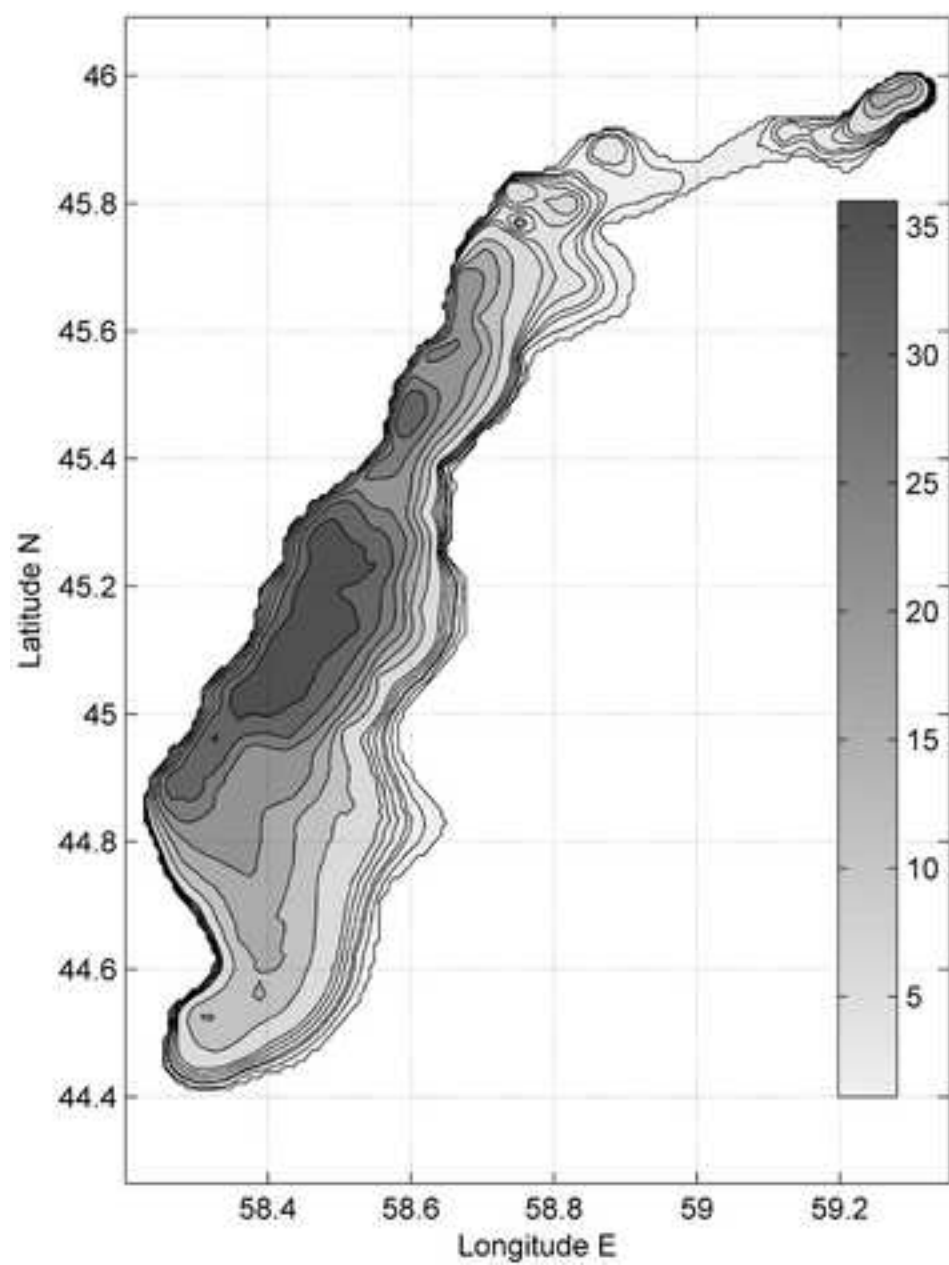


Figure7

[Click here to download high resolution image](#)

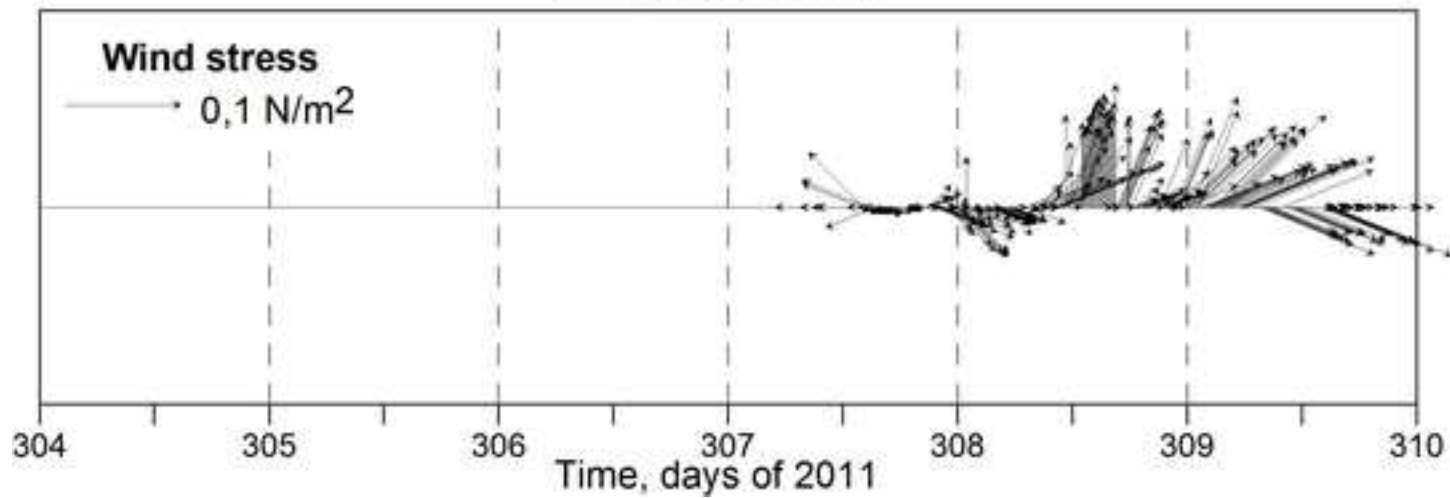
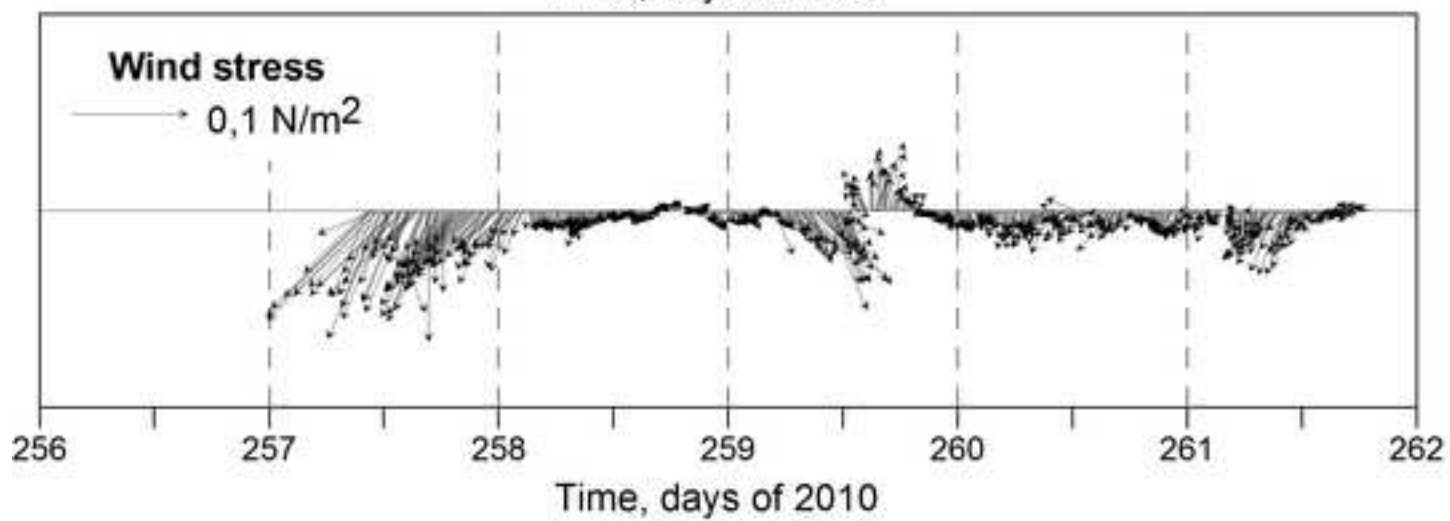
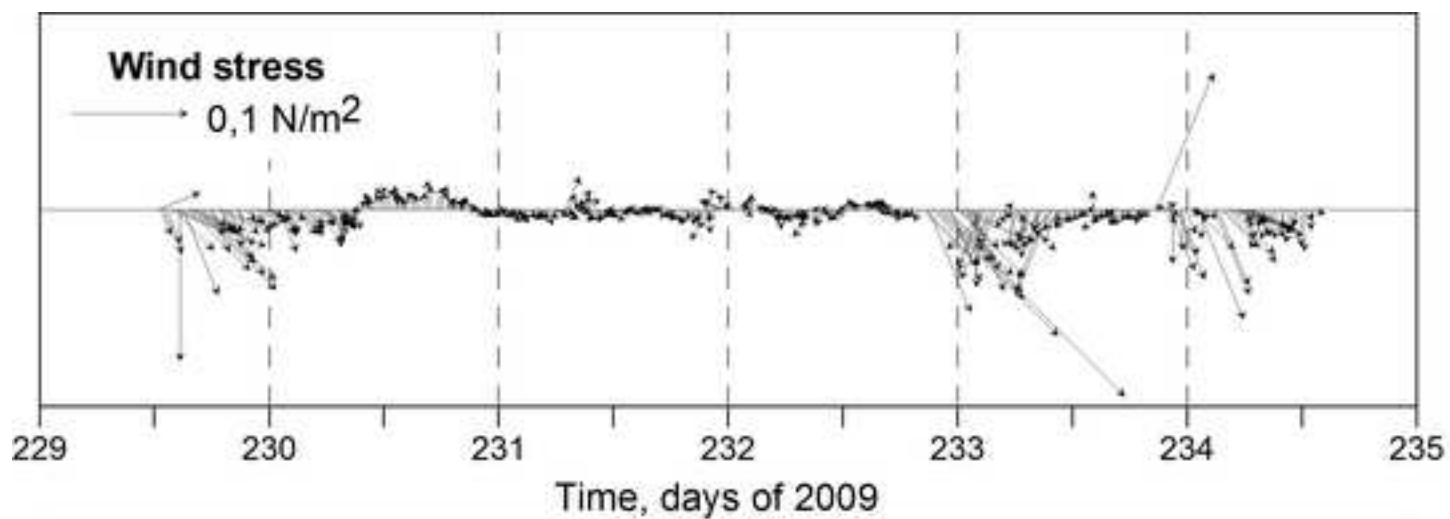


Figure8

[Click here to download high resolution image](#)

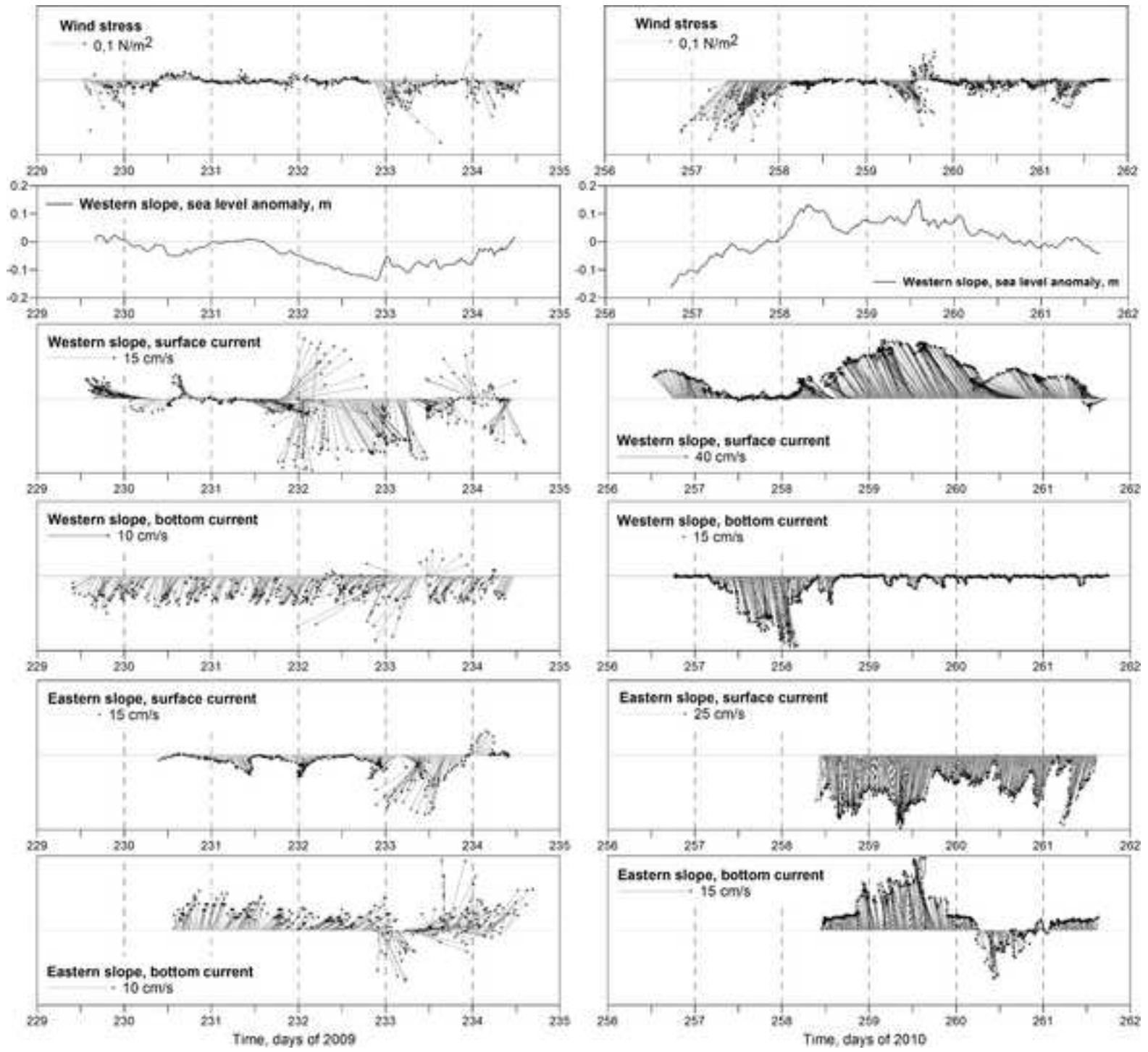


Figure9

[Click here to download high resolution image](#)

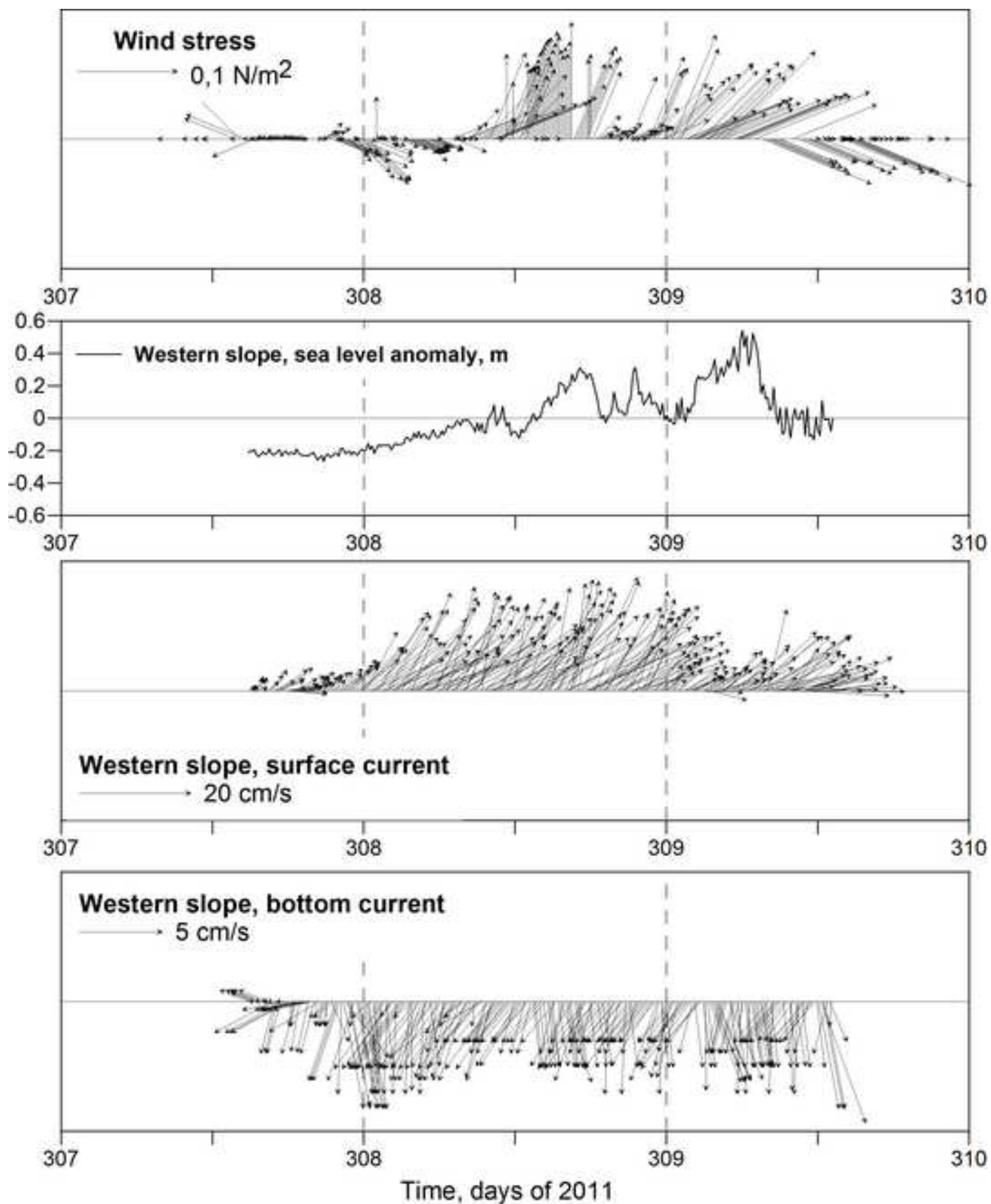


Figure10

[Click here to download high resolution image](#)

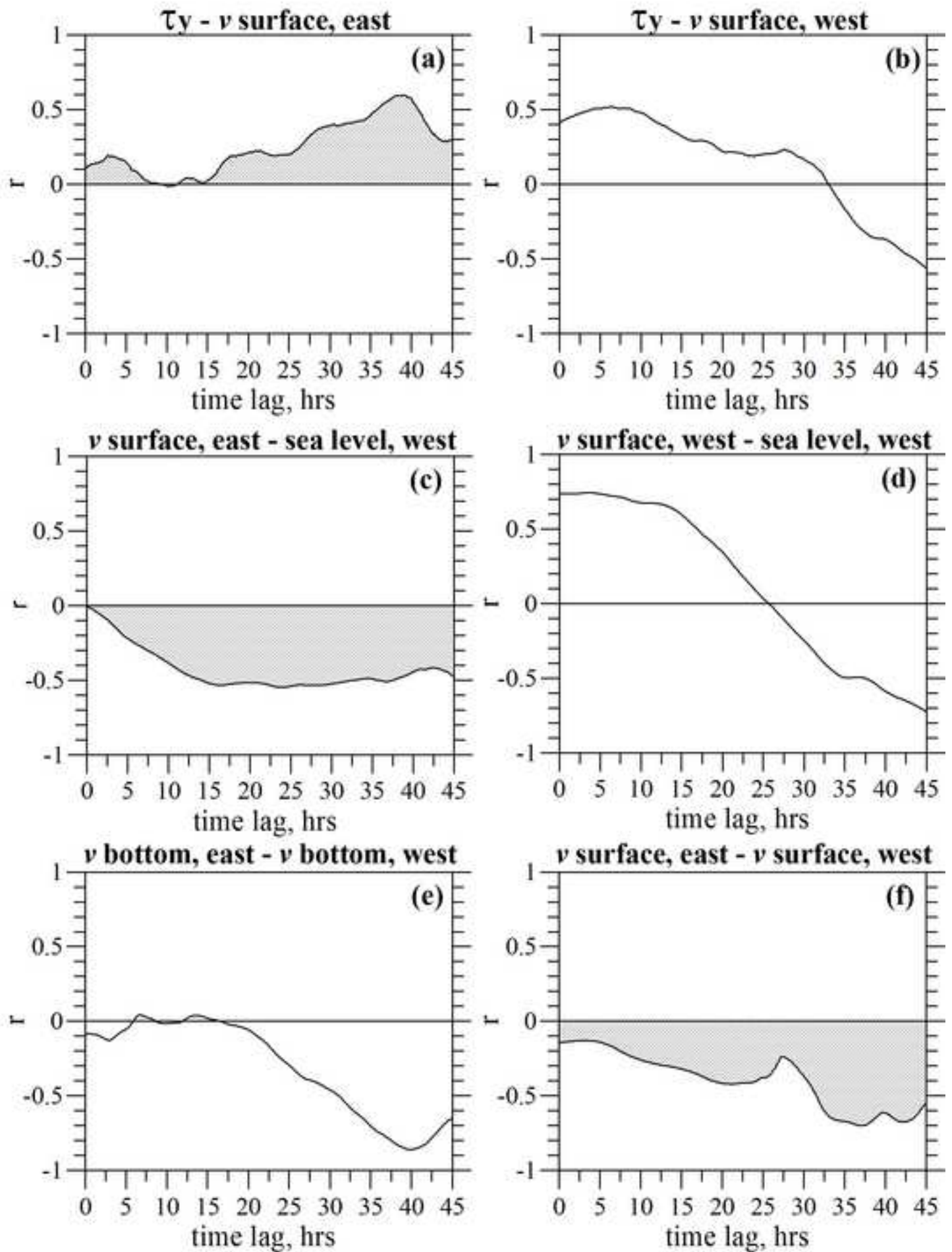


Figure11
[Click here to download high resolution image](#)

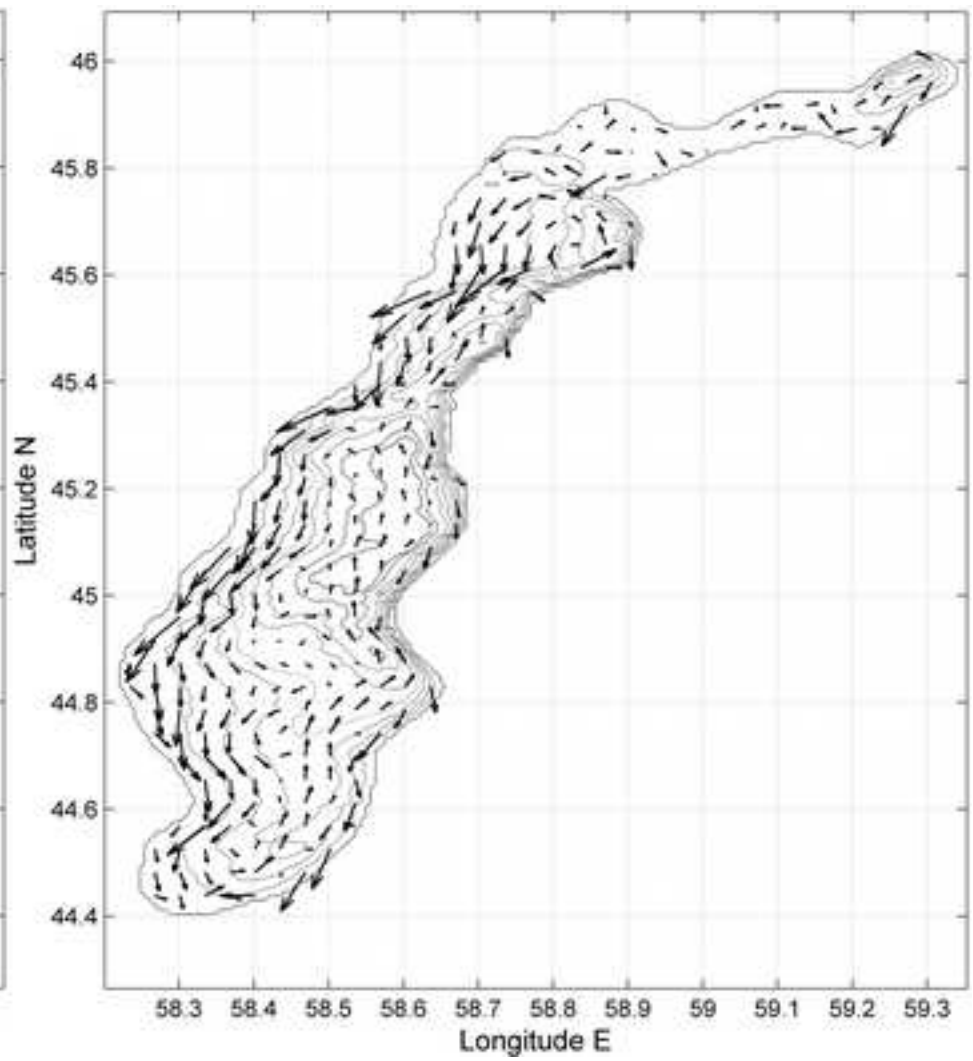
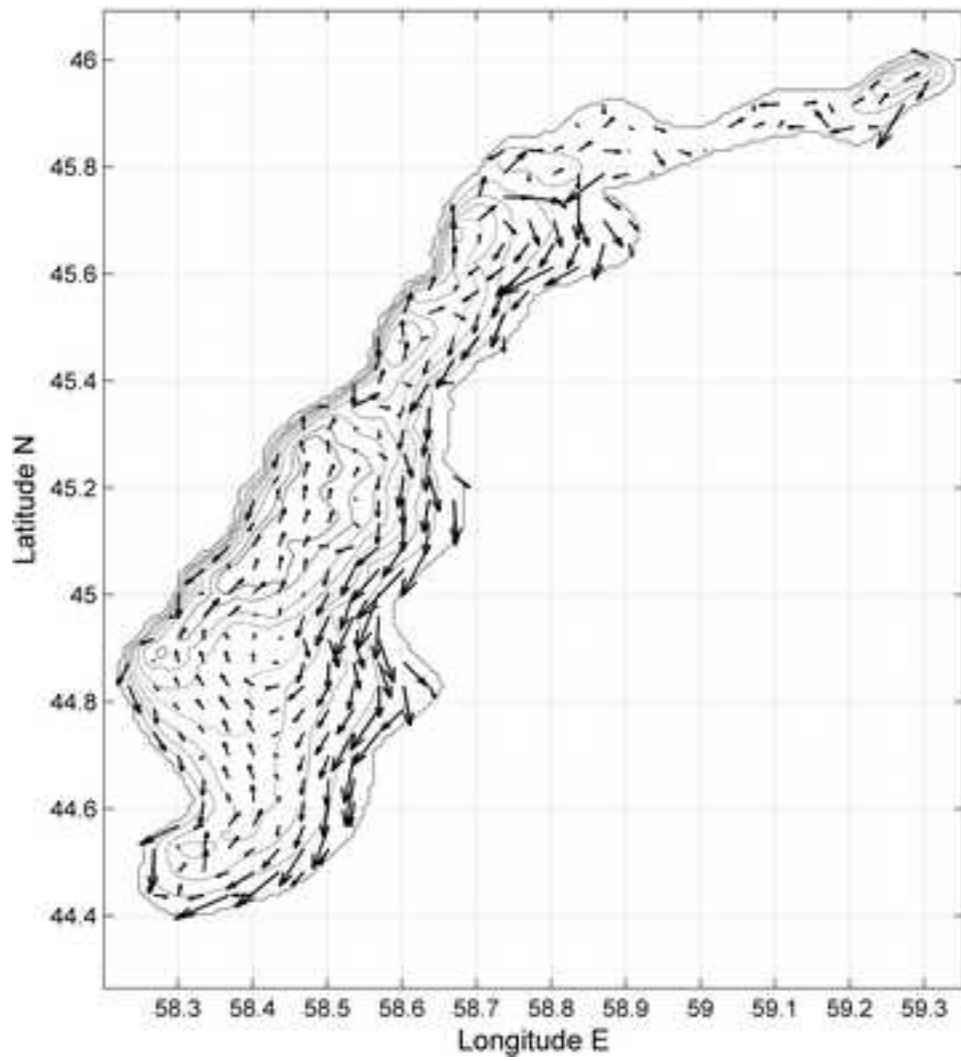


Figure12
[Click here to download high resolution image](#)

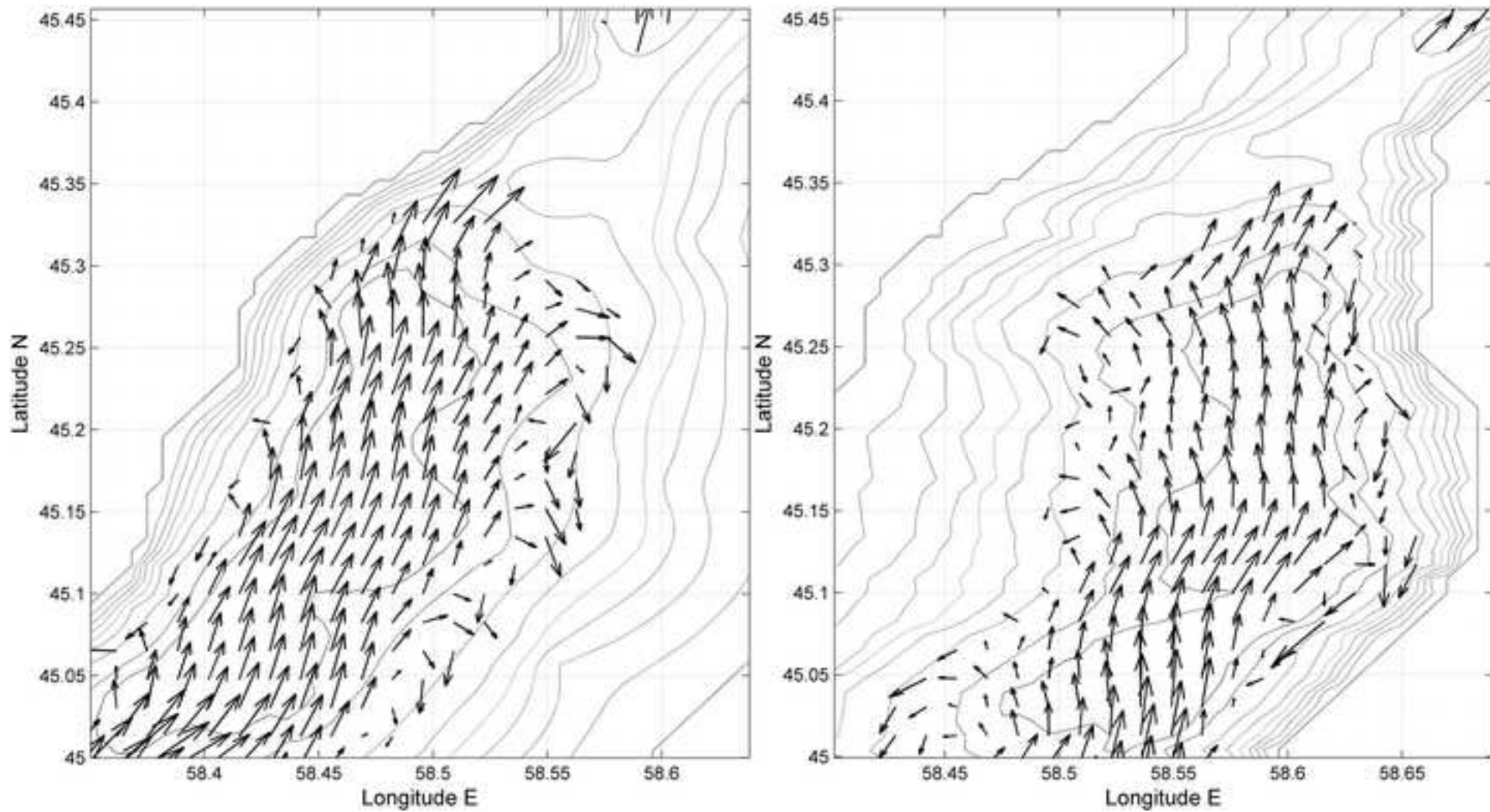


Figure13
[Click here to download high resolution image](#)

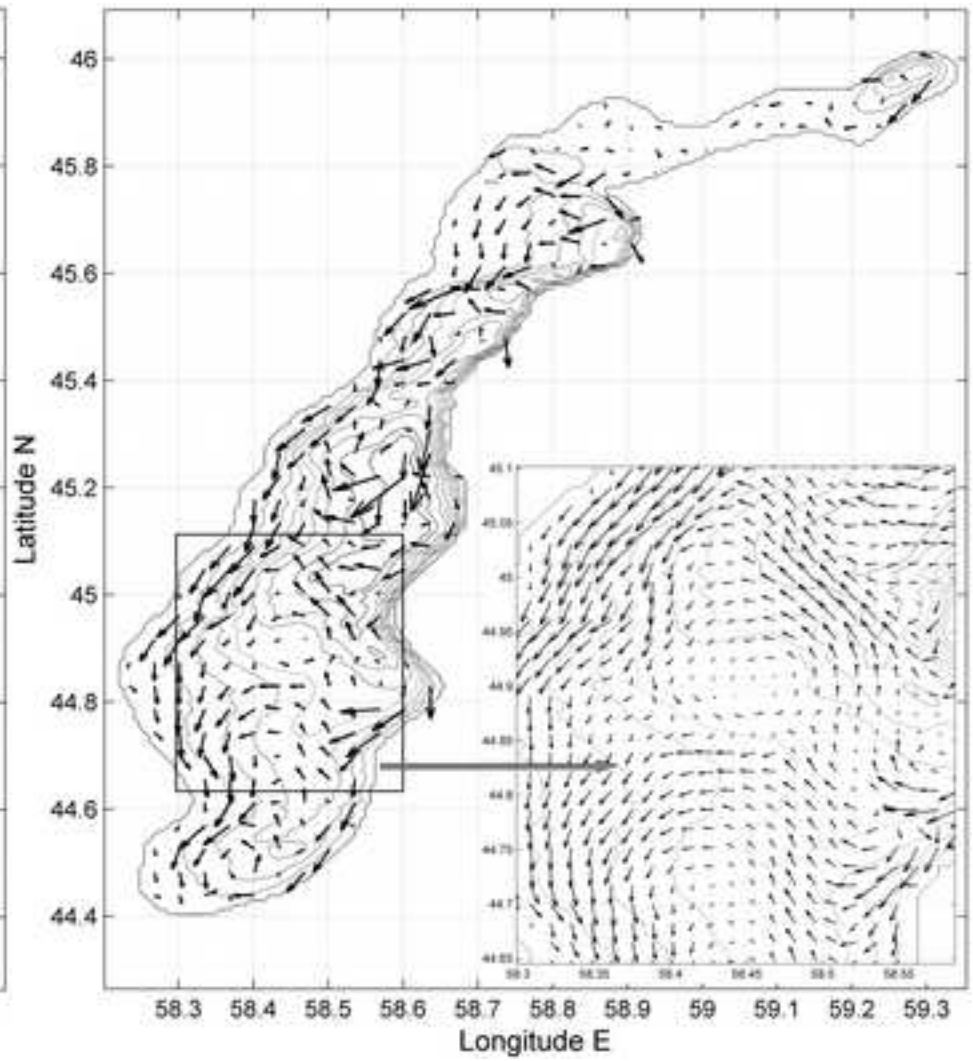
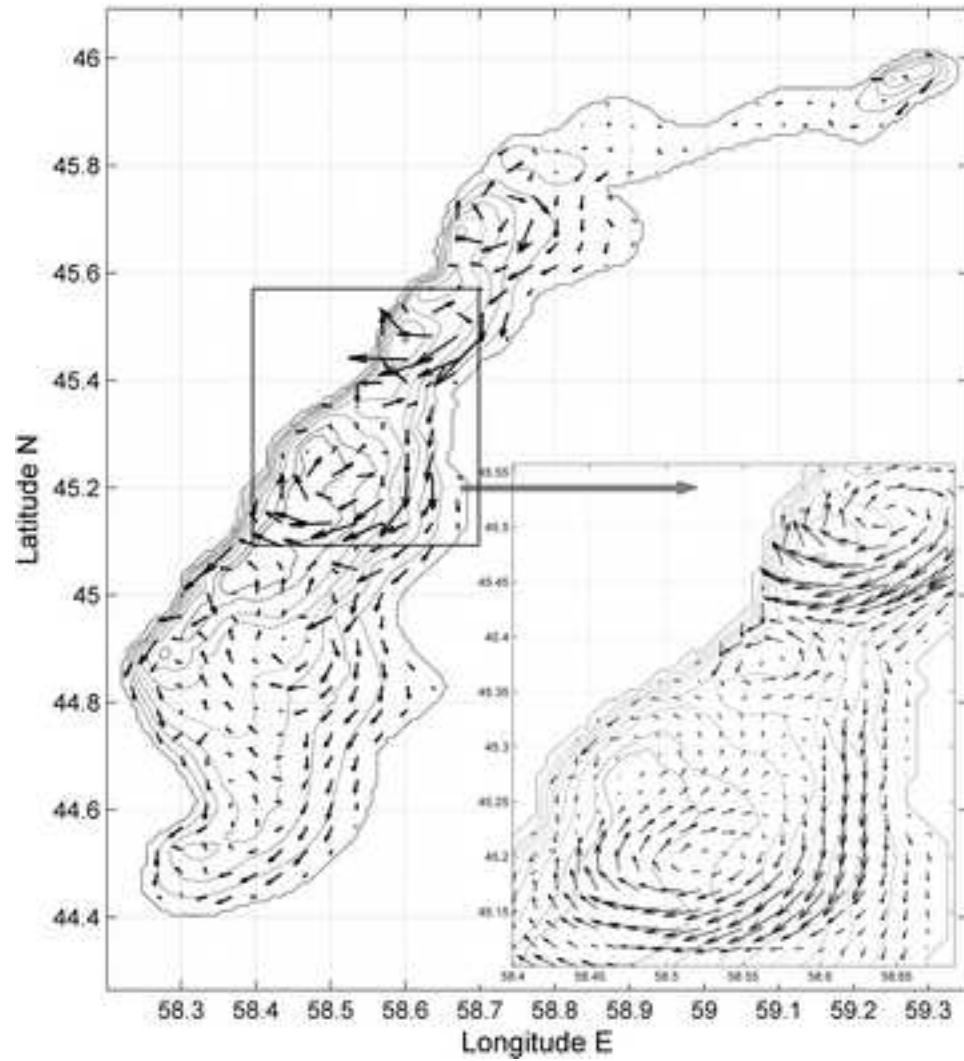


Figure14
[Click here to download high resolution image](#)

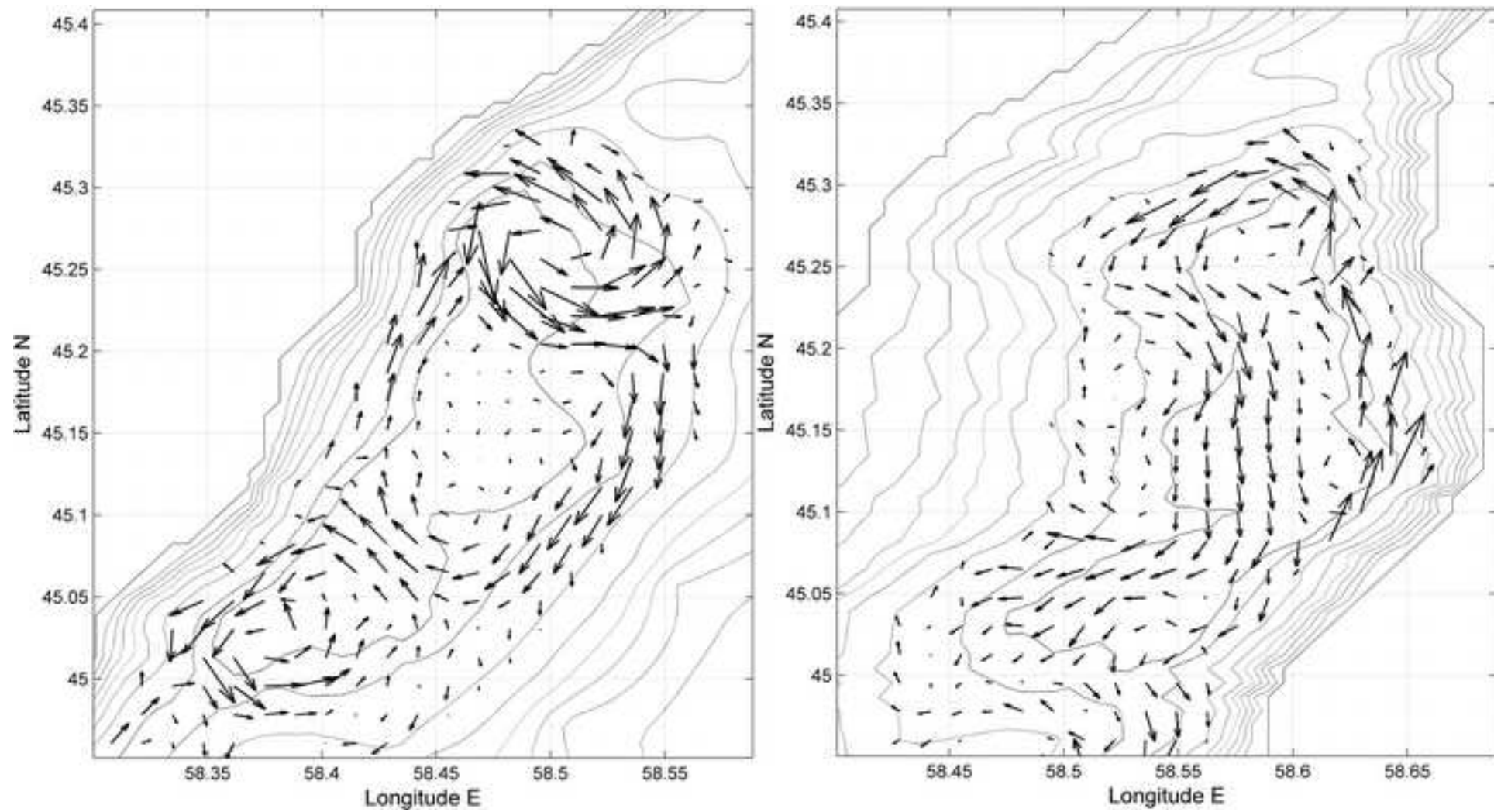


Figure1
[Click here to download high resolution image](#)

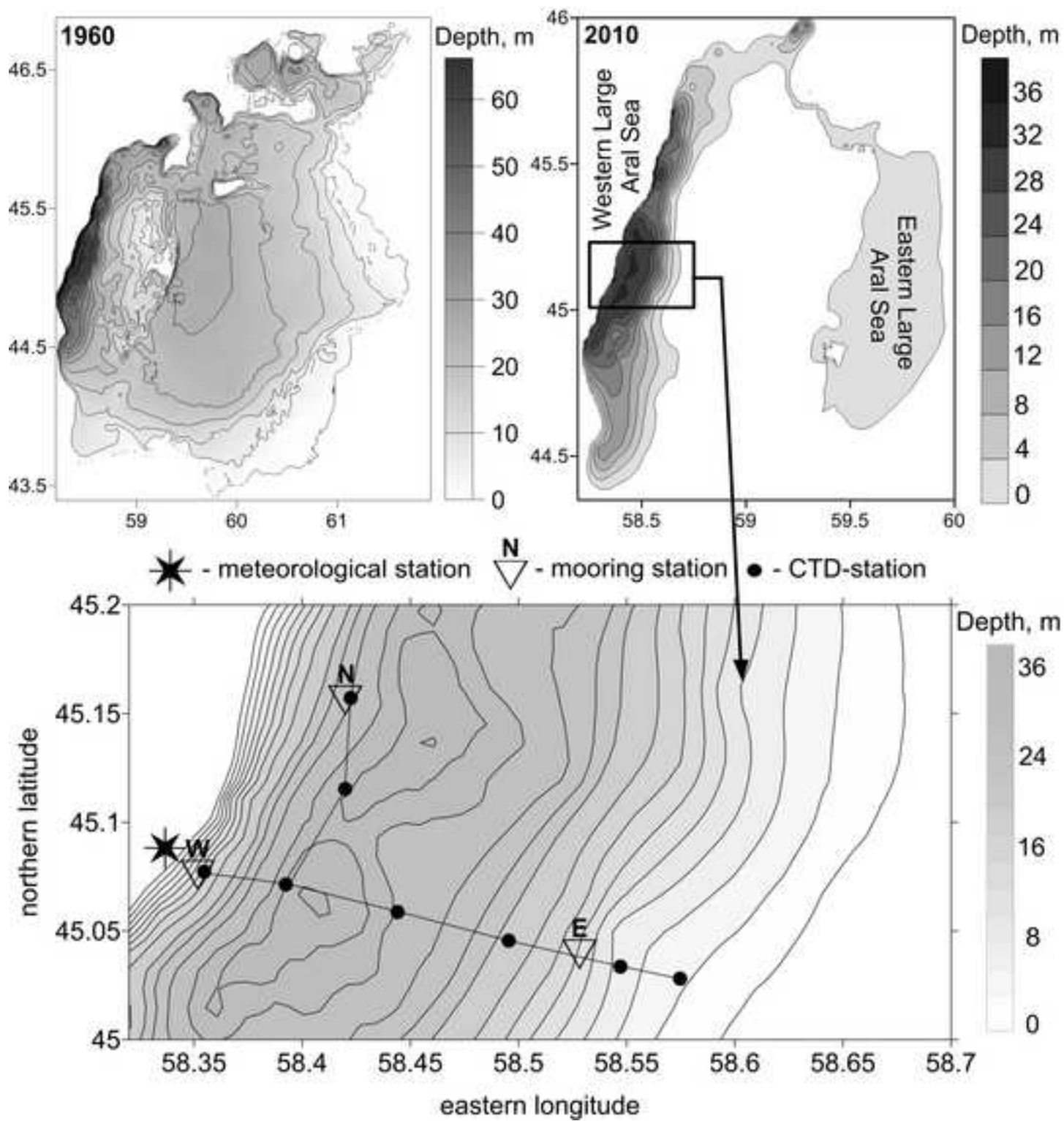


Figure3
[Click here to download high resolution image](#)

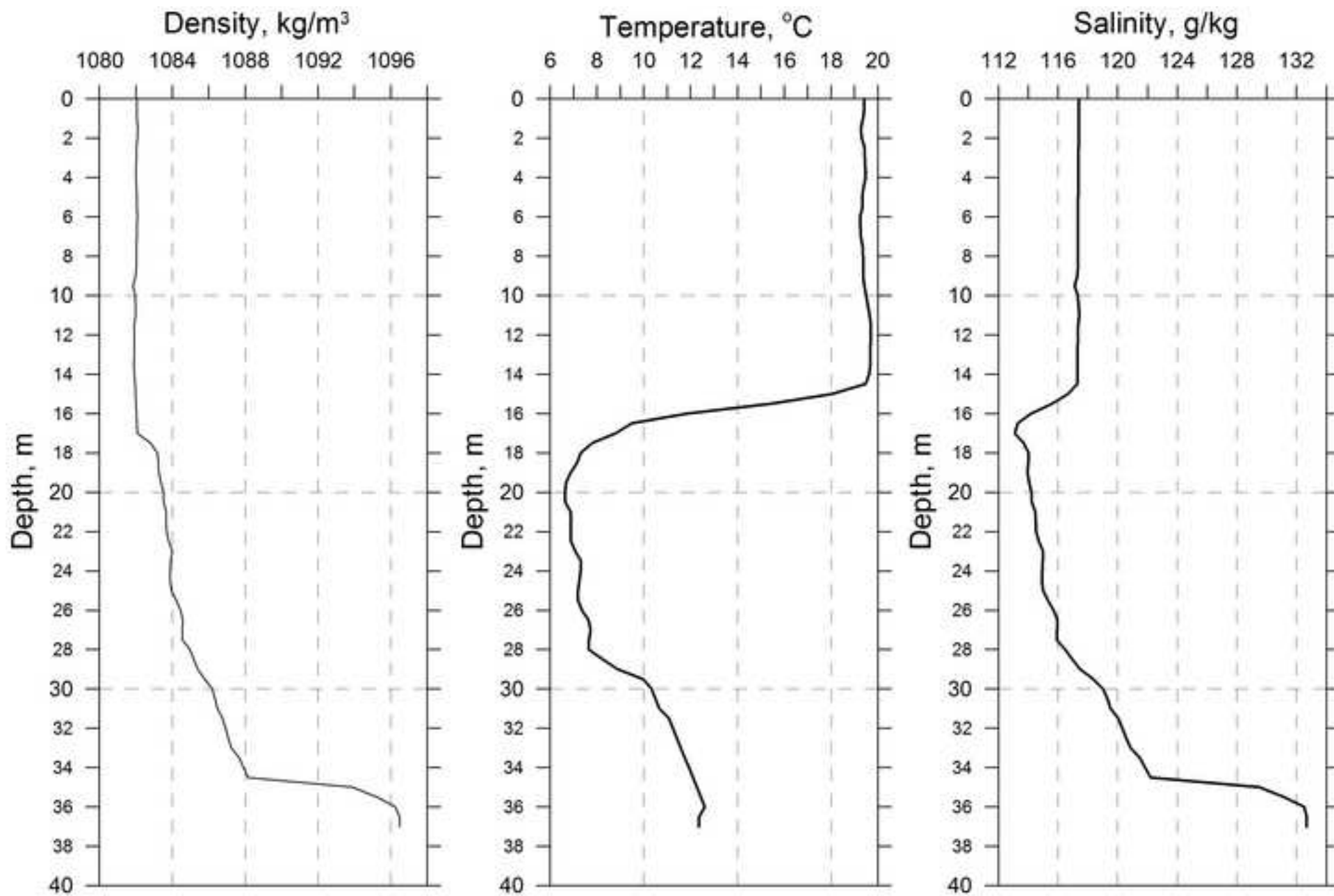


Figure4

[Click here to download high resolution image](#)

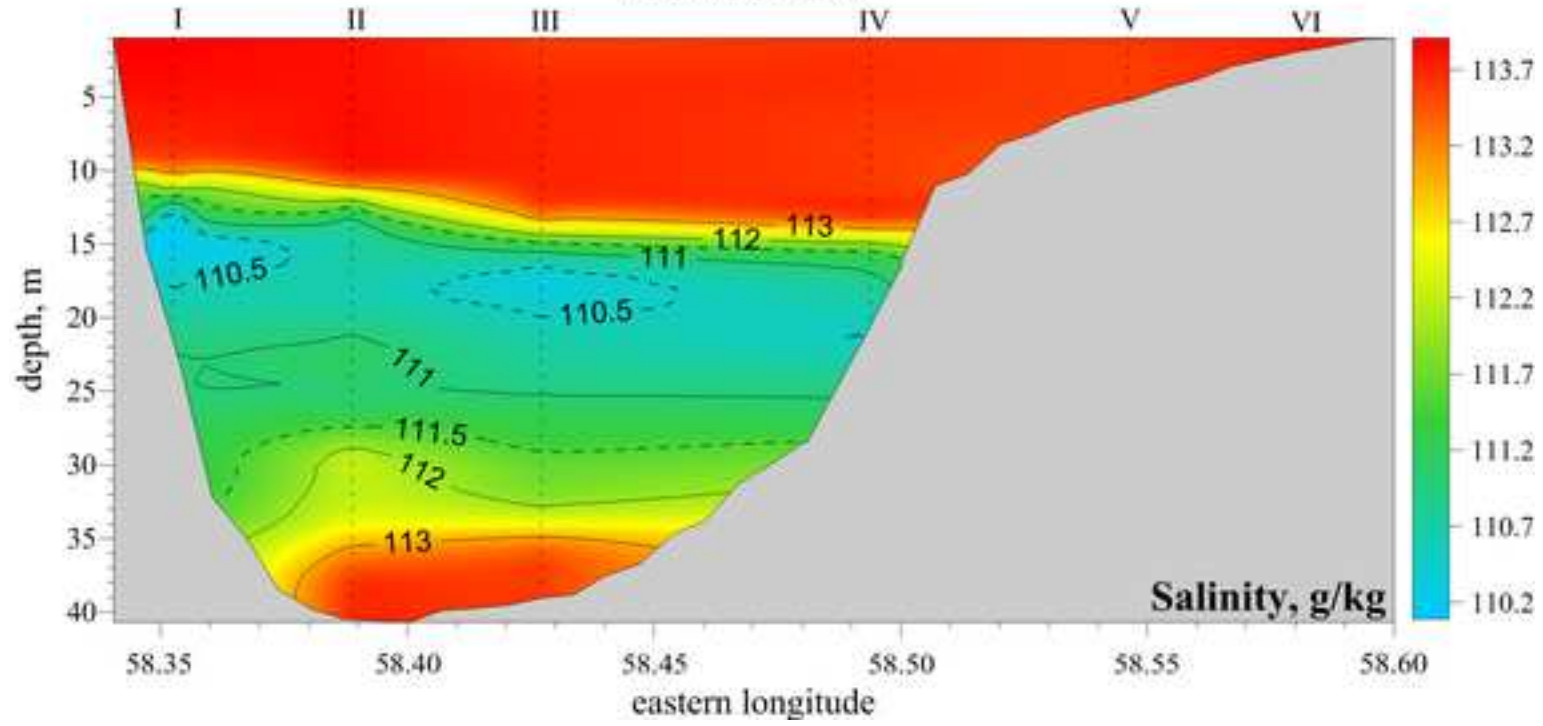
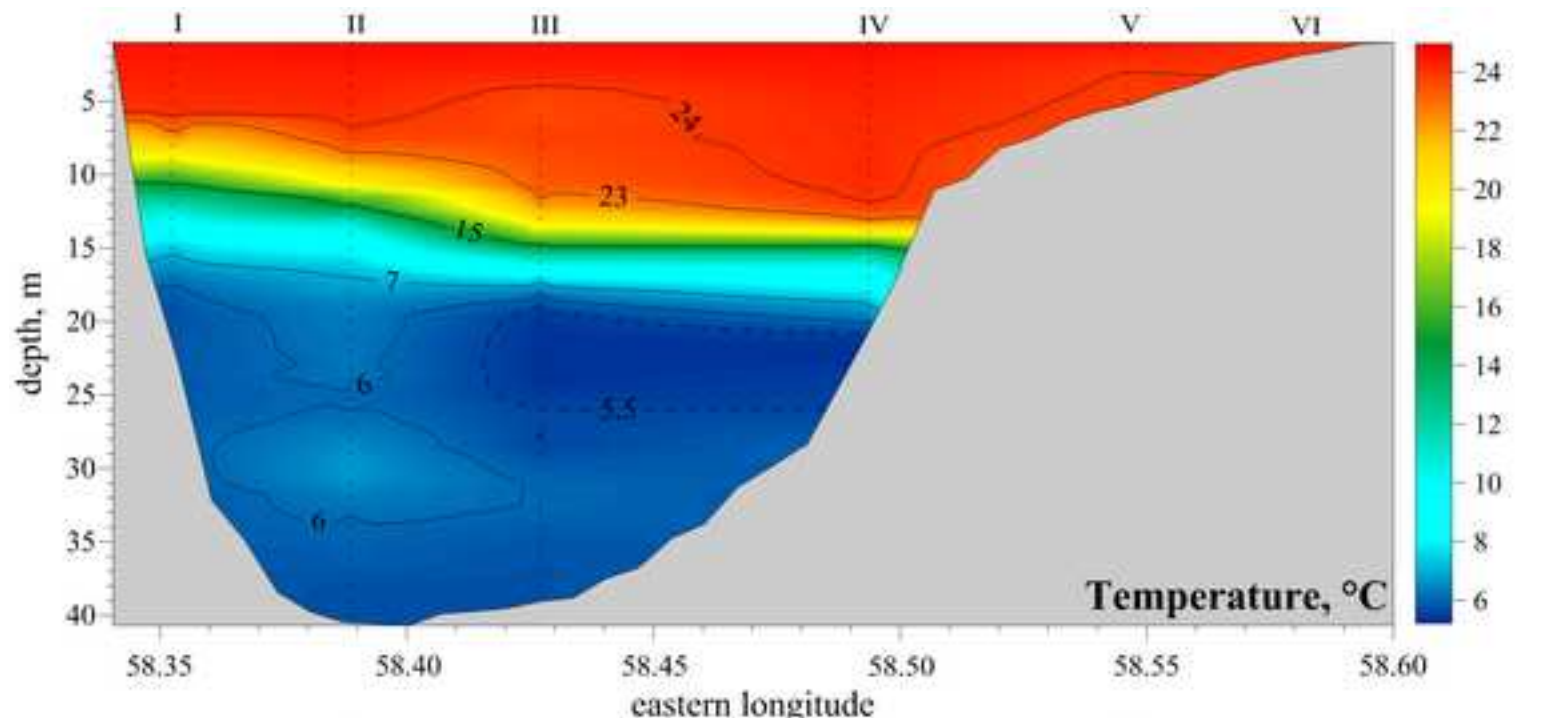


Figure5

[Click here to download high resolution image](#)

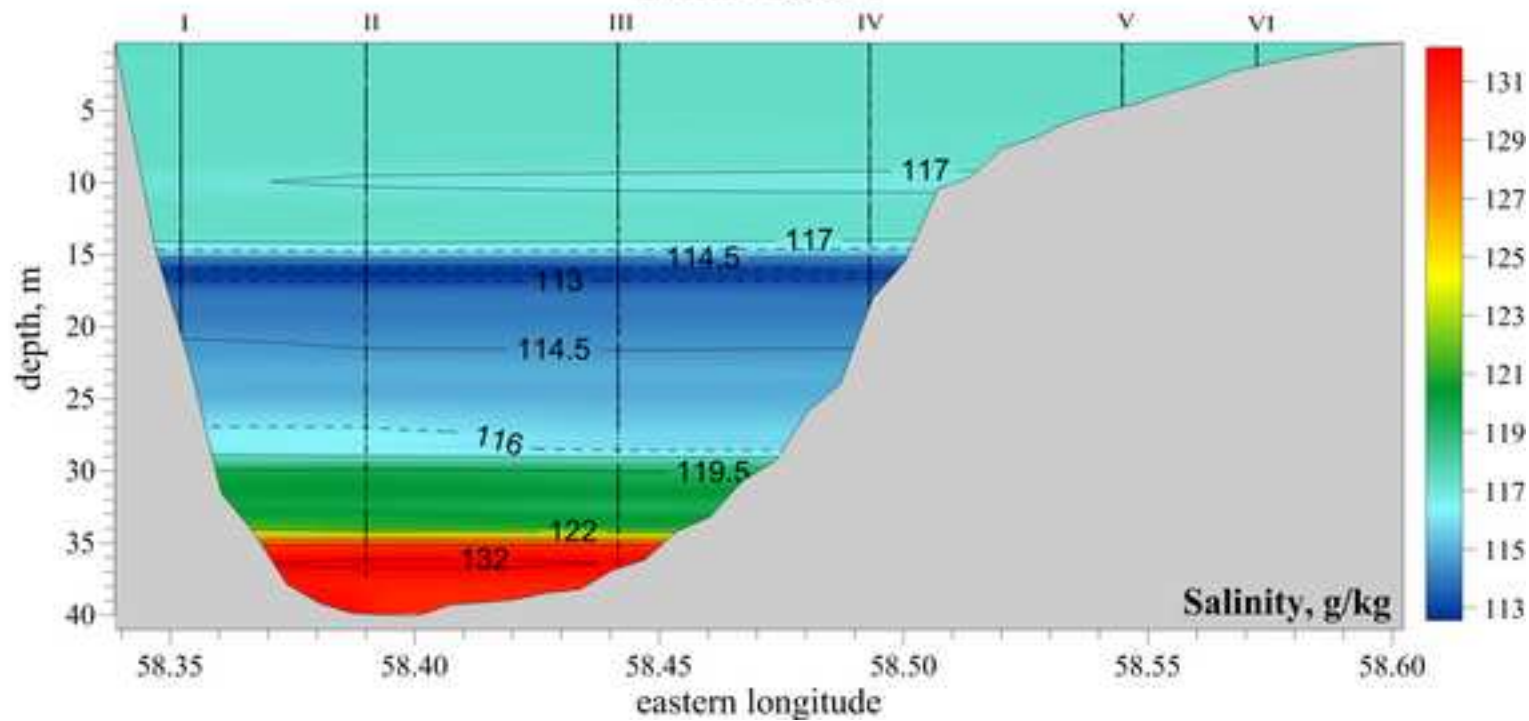
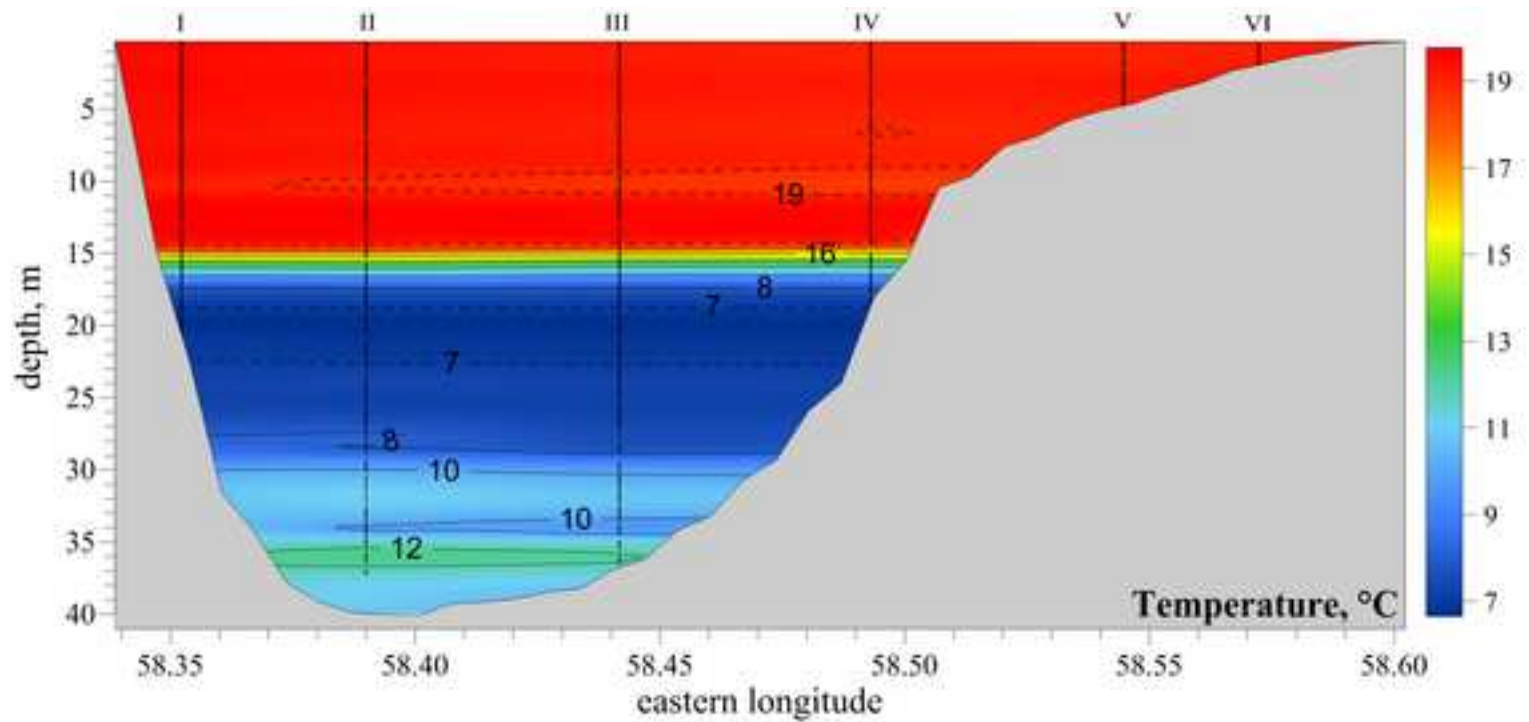


Figure6
[Click here to download high resolution image](#)

